



Arctic Ocean biogeochemistry in the high resolution FESOM 1.4-REcoM2 model



Vibe Schourup-Kristensen*, Claudia Wekerle, Dieter A. Wolf-Gladrow, Christoph Völker

Alfred-Wegener-Institut Helmholtz-Zentrum für Polar- und Meeresforschung, Am Handelshafen 12, 27570 Bremerhaven, Germany

ARTICLE INFO

Keywords:

Arctic Ocean
Marine primary productivity
Subsurface chlorophyll maxima
High resolution modeling
Unstructured mesh modeling
FESOM
REcoM2

ABSTRACT

In the rapidly changing Arctic Ocean, marine primary productivity is tightly linked to the balance between light and nutrient limitation. To capture this balance in ocean general circulation biogeochemical models (OGCBMs), a good representation of the physics is important due to the tight bio-physical coupling in the Arctic. Using a horizontal model resolution of a few kilometers makes it possible to resolve an increasing number of small scale processes, that otherwise need to be parameterized in OGCBMs. Such high resolution is, however, commonly not possible due to computational constraints. Utilizing an unstructured mesh approach, we have run the finite element sea-ice ocean model (FESOM 1.4) coupled to the biogeochemical model REcoM2 in a global configuration with an Arctic-wide resolution of 4.5 km. This resolution is so far unprecedented for a global biogeochemical setup, and here we present an analysis of the mean state of the model. FESOM-REcoM2's integrated Arctic net primary production (NPP) averages 445 Tg C yr^{-1} for the years 2011 to 2015, a value that is in the middle of the range compared to estimates from the literature. Most production takes place in the inflow regions of the Nordic and Chukchi Seas, and 32% is associated with the sea ice zone, the latter including the marginal ice zone and below-ice productivity. Light limits production to some degree at all latitudes north of 60°N , with growth becoming nutrient limited following the initial spring bloom in most places. The model reproduces the relatively low surface concentration of dissolved inorganic nitrogen (DIN) that has been observed in the central Arctic Ocean, as well as the low surface DIN concentration towards the end of the growth season further to the south, thereby also capturing widespread subsurface chlorophyll maxima (SCM). The SCMs are found in the whole Arctic except for the areas where sea ice concentration is high the whole year. They have a duration of two weeks to five months. The balance between nutrient and light limitations, both in the vertical and horizontal direction, highlights that decreased light limitation in a future ice free Arctic Ocean will not necessarily induce an increase in NPP due to increasing nutrient limitation, and that further studies of the role of the SCMs are required.

1. Introduction

With the rise in temperature over past decades, the Arctic Ocean is currently undergoing change that occurs faster than anywhere else on the planet. Most prominently, the extent of the summer sea-ice has decreased by approximately 30% over the past three decades (e.g. Stroeve et al., 2012), affecting the amount of solar radiation entering the water and the strength of the stratification (Davis et al., 2016), and thus also influencing the Arctic marine ecosystem (Wassmann, 2011).

Due to a relatively small number of *in situ* measurements in the Arctic Ocean, pan-Arctic estimates of net primary production (NPP) are most commonly based on satellite-based measurements (e.g. Pabi et al., 2008; Arrigo and van Dijken, 2015) or ocean general circulation biogeochemical models (OGCBMs, e.g. Zhang et al., 2010; Popova et al.,

2010; Jin et al., 2012). Currently, we do not know the exact magnitude of the Arctic Ocean NPP, but it is generally thought to be relatively low compared to global NPP (e.g. Sakshaug, 2004).

Marine primary producers are dependent on incoming photosynthetically available radiation (PAR) for photosynthesis. In the Arctic, the angle of the incoming PAR is low for most of the year, leading to a relatively low light intensity per area unit and a high degree of reflectance. The presence of sea ice further reduces the irradiance intensity through attenuation (e.g. Nicolaus et al., 2012). But as Arctic sea ice is becoming younger and thinner, the upper ocean light regime in the Arctic is changing (Perovich et al., 2011), with possible implications for the marine primary productivity. Ultimately, however, it is not light that controls the limits for seasonally integrated carbon uptake, but rather nutrient availability (Tremblay and Gagnon, 2009).

* Corresponding author.

Nitrate is thought to be the main limiting nutrient in the Arctic Ocean (Tremblay and Gagnon, 2009; Taylor et al., 2013b; Tremblay et al., 2015), though the limitation regime depends on for example the location, the time of the year and the phytoplankton composition (e.g. Sakshaug, 2004). In the summer, the melting sea ice induces a strong vertical stratification in the Arctic Ocean, thereby reducing the upward mixing of nutrients from deeper reservoirs, especially during the growing season (Randelhoff et al., 2016). Once nutrients have been depleted from the surface water, continued phytoplankton growth is thus dependent on sustained local supply of nutrients, e.g.; horizontal advection of nutrient rich water from the inflow regions (Carmack et al., 2006; Randelhoff et al., 2015), shelf break upwelling (Williams and Carmack, 2008) and riverine supply. An indication of the importance of nutrient availability late in the growth season in the Arctic, is the widespread occurrence of subsurface chlorophyll maxima (SCMs, Erga et al., 2014; Martin et al., 2012). The Arctic Ocean SCMs are characterized by a strong association with the nitracline, and act as barriers for upward nutrient transport through biological uptake (Martin et al., 2012). While the depth of the SCM is relatively shallow in the Arctic Ocean, studies from the Canada Basin indicate that the depth of the SCMs are in fact increasing due to the increased light availability, thereby pushing the surface ocean towards a more nutrient limited regime (Steiner et al., 2016).

For large scale OGCBMs, a good representation of the nutrient distribution is key in order to capture the seasonal progression between light and nutrient limitation in the area. Modeling a satisfying nutrient distribution is, however, something that has proven relatively difficult; while OGCBMs tend to agree on the distribution and strength of the NPP in the Arctic Ocean because of the strong dependence of NPP on the sea ice, the distribution and concentration of the nitrate shows large differences between different models (Popova et al., 2012). In order to use OGCBMs to understand how the Arctic Ocean productivity is affected by the physical changes, it is thus necessary to first assess the model's representation of the nutrient fields as well as the relative role that light and nutrients play for growth limitation. This is especially important as studies indicate that the role of nutrient limitation is likely to increase in the future (Popova et al., 2012; Vancoppenolle et al., 2013; Steiner et al., 2016).

One issue for large scale models is that a number of the processes providing nutrients to the surface ocean in the Arctic, such as upwelling and eddy transport, occur on a relatively small scale relative to the model's resolution. Such processes are thus commonly parameterized, and not well captured in models with a coarse resolution (McKiver et al., 2015). One way to optimize the representation of for example currents, mixing and heterogeneity of the sea ice in OGCBMs is therefore by increasing the resolution (Proshutinsky et al., 2011). In recent years, large efforts have been put into model runs with increased horizontal resolution; large scale OGCMs focussing on the Arctic Ocean have been run with a local horizontal resolution of up to 0.5–1 km (Chen et al., 2016; Hattermann et al., 2016; Wekerle et al., 2017a), thereby introducing the small-scale variability that is not captured in traditional models. Due to the increased computational demand introduced by biogeochemical modules, high resolution model runs including biogeochemistry have so far been carried out using regional models only; Wassmann et al. (2006) carried out a run with a nested domain of 4 km resolution in the Barents Sea, while Watanabe et al. (2014) used a regional model for the Arctic with a resolution of 5 km, both highlighting the importance of small scale variability for the biogeochemical representation. So far, however, nobody has run a coupled biogeochemical model in a global setup with such a high resolution in the whole Arctic Ocean.

By utilizing an unstructured mesh approach, Wekerle et al. (2017b) recently carried out a global model run with an Arctic-wide resolution of 4.5 km, thereby improving the mean flow and introducing a significantly larger spatial variability compared to a control run with a 24 km resolution. In the current study, we further advance this run by

introducing the biogeochemical module REcoM2 to the setup of the Finite Element Sea-ice Ocean Model (FESOM). Here, we evaluate the performance of the model with respect to light, nutrients, chlorophyll and net primary productivity by comparing to relevant observational data sets. Further, we analyze the relative importance of light and nutrients for the models' productivity, and demonstrate a widespread SCM.

2. Model description and simulations

2.1. Ocean general circulation model

For the current study we were using the Finite Element Sea-ice Ocean Model (FESOM) version 1.4 (Wang et al., 2014) coupled to the biogeochemical model REcoM2 (Hauck et al., 2013; Schourup-Kristensen et al., 2014). FESOM is a global sea-ice ocean model, which solves the primitive equations under the commonly applied Boussinesq approximations using the finite element method. FESOM 1.4 is an update from the version used in previous work with REcoM2 (Schourup-Kristensen et al., 2014). Important improvements include a change of the parameterization of the diapycnal mixing from the Pacanowski-Philander parameterization (PP, Pacanowski and Philander, 1981) to the *k*-profile parameterization (KPP, Large et al., 1994). This ensures that vertical turbulent mixing occurs to a larger degree when the water column is stably stratified. Due to the variable horizontal grid resolution of the model run, the isopycnal, diapycnal and vertical diffusivity are scaled to the resolution, under the assumption that resolved eddies will be responsible for a larger part of the transport when resolution is increased. A full description of the current model version can be found in Wang et al. (2014).

2.2. Biogeochemical model

The biogeochemical model REcoM2 was originally developed by Schartau et al. (2007) for mesocosm studies, and has since been further developed for large scale studies and coupled to FESOM (Schourup-Kristensen et al., 2014). In our setup, REcoM2 describes one class of zooplankton, two classes of phytoplankton, the nutrients nitrogen, silicon and iron, as well as the carbon cycle. A full description of REcoM2 can be found in Schourup-Kristensen et al. (2014). REcoM2 has so far mainly been used for studies focussing on the Southern Ocean (e.g. Taylor et al., 2013a; Losch et al., 2014; Hauck and Völker, 2015) and the current study is thus the first with REcoM2 focussing on the Arctic Ocean.

In the Arctic Ocean riverine input of nitrogen and silicon plays a role for biological productivity, especially in the vicinity of river mouths, and has thus been added to the model code along with aeolian deposition of dissolved inorganic nitrogen (DIN). Riverine input of DIN, dissolved inorganic silicon (DSi) and organic nitrogen (DON) is added from the model based database Global NEWS version 2 (Mayorga et al., 2010; Beusen et al., 2009). This database provides a constant nutrient flux to the ocean from the major world rivers. Nitrate is further added to the surface water through aeolian input using global 10-year mean fields from from 1850 to 2000 (Lamarque et al., 2010). In REcoM2, the effect of sea ice coverage on PAR is taken into account by scaling the surface PAR linearly with the fraction of open water in a given node, thereby neglecting the fraction of PAR that penetrates the sea ice directly.

2.3. Simulations

For the current study we have performed a simulation using FESOM-REcoM2 in a global setup with increased horizontal resolution in the Arctic region; the resolution north of 60°N equals 4.5 km, between 40 and 60°N it is approximately 25 km, while a resolution of nominal 1° is used south of 40°N (Fig. 1a). The Rossby radius of deformation, which

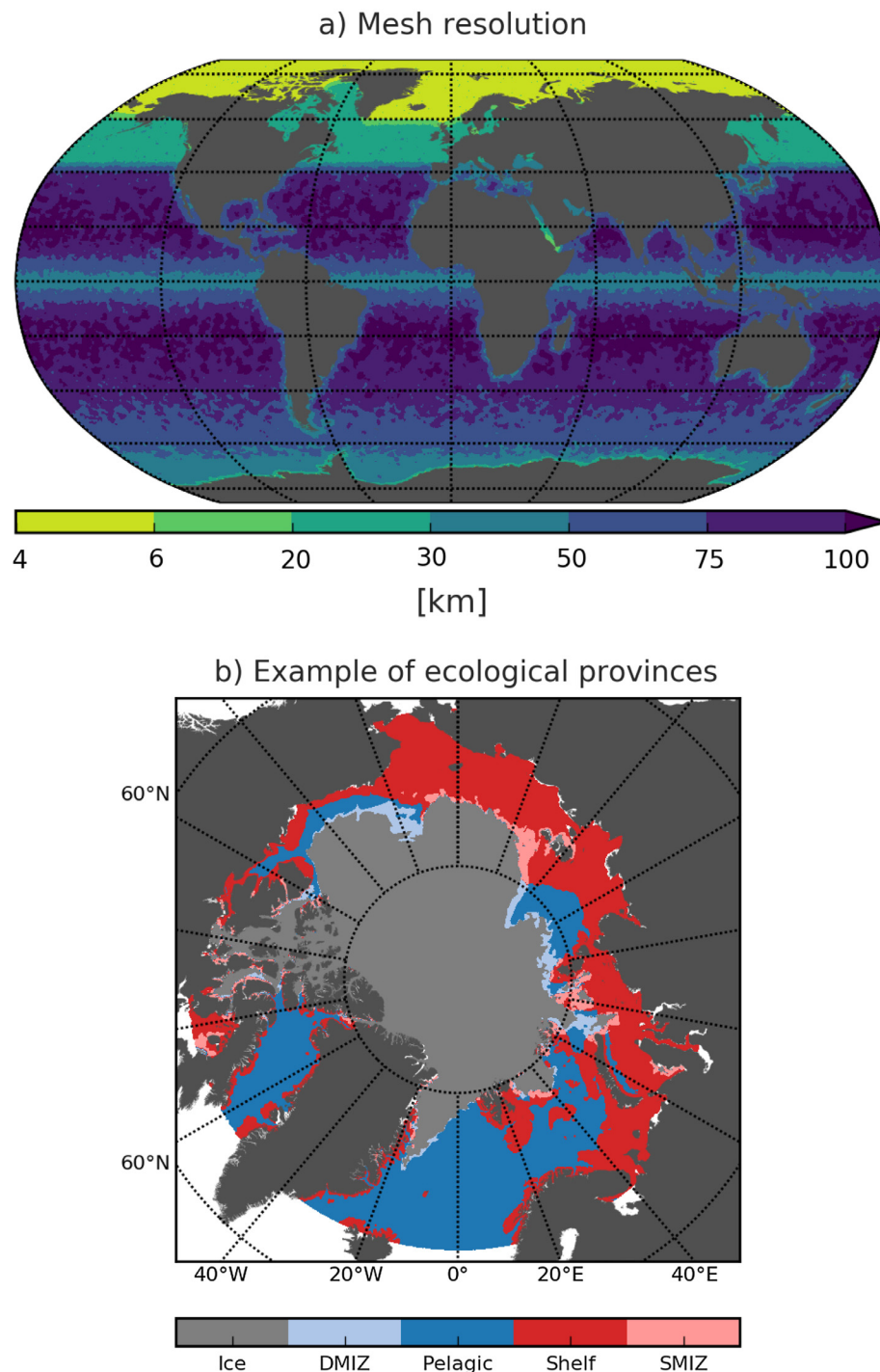


Fig. 1. (a) Horizontal resolution of the mesh used in our study. (b) Example of the division of the Arctic Ocean into ecological zones on the 15th of August 2014.

gives an indication of the resolution needed to resolve eddies, is relatively small and variable in the Arctic Ocean (Nurser and Bacon, 2014). Comparing to the size of the Rossby radius of deformation, the grid is eddy permitting in the Nordic Seas, eddy resolving in the deep central Arctic Ocean, especially in the Canada Basin, and not eddy resolving on the shelves (Wekerle et al., 2017b, their Fig. 2c). In the vertical, the resolution is ten meters in the upper 100 meters of the water column, after which it increases with depth. The surface layer is located at 0 meters.

The coupled model run was started in the year 1980 and ended in 2015. The run was forced by the Japanese reanalysis dataset (Japan Meteorological Agency, 2013, accessed March 2016, JRA55). Prior to

starting the biogeochemical model, FESOM had done 40 years of spin-up under the CORE-II forcing (Large and Yeager, 2008), starting in the year 1958 and ending in 2009. The ocean state for this run has been comprehensively described by Wekerle et al. (2017b). Initializing FESOM with the final state from Wekerle et al. (2017b) means that the first ten years of our 36-year run should be considered spin-up.

In the biogeochemical model REcoM2, the macronutrients DIN and DSI were initialized from World Ocean Atlas 2005 (Garcia et al., 2006) and the dissolved inorganic carbon (DIC) and alkalinity was initialized using the GLODAP database (Key et al., 2004). Due to scarcity of iron measurements, no global field exists for dissolved iron concentrations, and the model's iron concentration was therefore initialized with an

output file from the Pelagic Interaction Scheme for Carbon and Ecosystem Studies model (NEMO-PISCES, [Aumont and Bopp, 2006](#)). All other tracers were initialized using very small values.

Here we analyze the last five years of the run, 2011 to 2015 using model output that was saved every second day. For animations, we show results from the year 2015, the last year of the simulation.

2.4. Geographical and ecological zones

We define the Arctic Ocean (AO) as the area north of the Polar Circle located at $66^{\circ}33'N$. For most analyses, we look at the pan-Arctic distribution of parameters, but as polar biological productivity is tightly coupled to the presence of sea-ice, we divide the Arctic into five ecological zones based on the depth of the water and sea-ice distribution following [Pabi et al. \(2008\)](#) and [Arrigo et al. \(2008\)](#), but introducing a fifth zone for the under ice productivity. The four ecological zones are defined as follows; the Pelagic and ice free shelf zones are characterized by not having had ice coverage in the past 14 days, the Pelagic Zone has a water depth larger than 220 m and the Ice Free Shelf Zone has a depth equal to or less than 220 m. The marginal ice zone (MIZ) is defined as the area that has no ice cover at the present day, but has had ice cover in the past 14 days. The MIZ is divided into the pelagic and shelf marginal ice zone (DMIZ and SMIZ), based on depth as in the open water zones. In the model a point is considered open water when the ice concentration is lower than 10% following [Arrigo et al. \(2008\)](#). The ecological zones thus change with time. An example of the distribution on the 15th of August is plotted in [Fig. 1b](#).

2.5. Data

To assess the model results against measured data, we need datasets of relevant parameters with a relatively good spatial and temporal coverage for the Arctic Ocean. In this study we focus on sea-ice concentration, surface DIN and DSI, surface chlorophyll *a* and vertically integrated NPP.

For sea ice concentration we use satellite-based estimates from the National Snow and Ice Data Center (NSIDC, [Cavalieri et al., 1996, updated yearly, accessed 15.03.17](#)). These provide pan-Arctic values for the whole year on a daily basis. We use this to evaluate FESOM's ice concentration as well as the number of ice free days in the model.

For the nutrients DIN and DSI we have to rely on *in situ* measurements, which are relatively sparse in large parts of the Arctic Ocean due to its inaccessibility. Here, we use the World Ocean Atlas 2013 (WOA13, [Garcia et al., 2014](#)), which provides a global gridded representation of nutrient distributions, including the Arctic Ocean. One problem, however, is that while a relatively large number of measurements of nutrient concentrations have been carried out in the more accessible regions such as the Greenland, Barents and Chukchi Seas, other regions are not well represented. The central Arctic is especially heavily interpolated. For this reason we have chosen to show only the regions in which data exists, and have masked out regions without data. Additionally, we show both the modeled mean surface nutrient distributions, which we define to be the average of the surface nutrient concentrations for the years 2011 to 2015, as well as the minimum and maximum concentrations. In order to assess how realistic the latter fields are, we also compare them to *in situ* pre- and postbloom concentrations in the discussion.

We use large scale fields of chlorophyll (Globcolour, <http://globcolour.info>) and NPP (CbPM, [Behrenfeld, 2005](#); [Westberry et al., 2008](#)) calculated from satellite-based estimates of ocean color. Both fields have a spatial resolution of approximately 4 km. The chlorophyll is given as daily composites and the NPP as 8-daily. Ocean color measurements are dependent on light and can thus only provide values for open water and for the summer period. To get as full a coverage as possible we compare the modeled and satellite-based estimates of chlorophyll and NPP for the five month summer period from May 1st to

September 30th. This period entails the spring bloom in the Nordic Seas as well as the summer bloom in the central Arctic, and does therefore capture the most important biological season well. When comparing model output to satellite-based estimates of chlorophyll and NPP it is important to note that these are not direct measurements, but rather another type of model that converts measurements of ocean color to chlorophyll and NPP through a number of assumptions regarding for example mixed layer depth and the subsurface profile of phytoplankton carbon (e.g. [Behrenfeld and Falkowski, 1997](#); [Carr et al., 2006](#)). Consequently the following must be kept in mind when comparing satellite-based estimates of chlorophyll and NPP to model results: (1) The number of measurements in each pixel is relatively low as they are dependent on the path of the satellite, and are disturbed by the presence of sea ice and clouds. (2) The algorithm used to calculate the chlorophyll concentration is developed for blue water conditions, which is problematic in the optically complex Arctic waters ([Wang, 2005](#)), leading to an overestimation of coastal chlorophyll ([Matsuoka et al., 2007](#); [Chaves et al., 2015](#)). (3) The measured chlorophyll concentration covers a non-specified depth range; in clear water they may reflect deeper chlorophyll than in more turbid water, and it is not clear to what extent SCMs are recorded ([Arrigo et al., 2011](#); [Hill et al., 2013](#)). Nevertheless, the satellite-based estimates gives an impression of the large scale distribution of productivity, and can be used to compare with the model's productivity.

3. Results

3.1. Ice and light

For the years 2011 to 2015, the average modeled September sea ice extent sums up to $5.6 \pm 0.53 \cdot 10^6 \text{ km}^2$ as compared to $5.3 \pm 0.61 \cdot 10^6 \text{ km}^2$ for the satellite-based estimate ([Cavalieri et al., 1996, updated yearly, accessed 15.03.17](#)).

FESOM's September sea ice concentration (fraction between 0 and 1) is highest in the area north of Greenland and of the Canadian Arctic Archipelago (CAA), while the Russian and Canadian shelves are ice free ([Fig. 2a](#)). This distribution fits well with the satellite-based estimates ([Fig. 2b](#)), and with the well established knowledge that multi-year ice foremost is found north of the CAA, while first-year ice can be found to a higher degree in the inflow regions and on the Siberian shelves (e.g. [Comiso, 2012](#)). The minimum sea ice extent is on average slightly overestimated in FESOM, mainly due to too much ice in the Beaufort Sea. Looking more into detail of the modeled sea ice, the Barents, Kara and Laptev Seas are largely ice free up to $80^{\circ}N$ in both FESOM and the satellite-based estimates, while the ice edge is located closer to the coast in the East Siberian Sea ([Fig. 2](#)). In the Chukchi and Beaufort Seas as well as the CAA, FESOM's ice extent is somewhat overestimated compared to the satellite-based values. The interannual variability of the minimum sea ice extent is well captured in FESOM (e.g. [Wekerle et al., 2013](#); [Wang et al., 2016b](#)), partly due to the strong dependence of the sea ice on the atmospheric forcing. This means that the mean sea-ice extent varies from 2011 to 2015, with the lowest extent occurring in 2012 (Not shown).

The model resolution of 4.5 km means that FESOM reproduces larger spatial heterogeneity in terms of sea ice than what is the case in coarser models ([Wang et al., 2016a](#)). The spatial heterogeneity, including large scale leads and localized areas of thinner sea ice, is especially clear in animations of the bi-daily sea ice concentration ([Fig. 3](#)), but can also be seen north of Greenland in the mean September sea ice concentration ([Fig. 2](#) and [A.14](#)). This is a feature that modulates the strength of the PAR below the ice and thus has an impact on the modeled biological productivity as it affects the amount of light that reaches the surface water, as will be discussed in [Section 4.4](#). While a full analysis of the mesoscale processes on the productivity is beyond the scope of the current study, it is likely that these processes will become more important in the future when the Arctic becomes ice free to

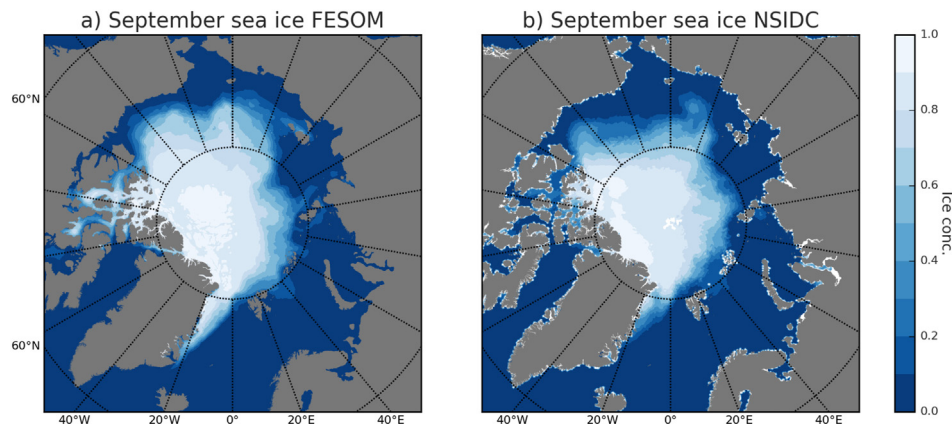


Fig. 2. September mean sea ice concentration for 2011 to 2015 in (a) FESOM and (b) satellite-based estimates from NSIDC (Cavalieri et al., 1996).

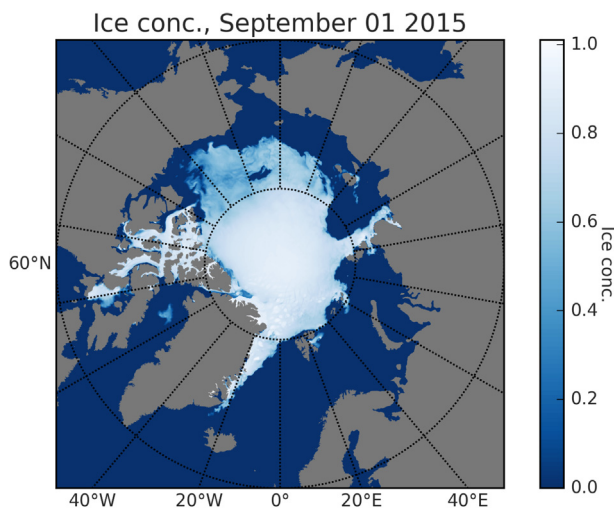


Fig. 3. Placeholder for the animation “FESOM-REcoM2_IceConc2015.mp4” submitted as supplementary material: An animation of the spatial distribution of the modeled sea ice concentration as it develops for the year 2015.

a larger degree.

The attenuation effect of the sea ice significantly reduces the amount of irradiance reaching the water. The transmittance in FESOM-REcoM2 is scaled to the fraction of open water in a given node, and the growth in the surface water is thus dependent on a correct representation of the sea ice retreat and number of ice free days in the Arctic. The satellite-based data (Cavalieri et al., 1996, updated yearly, accessed 15.03.17) shows that most of the Nordic Seas and the Barents Sea are ice free the whole year, while the shelves north of Russia and in the Chukchi Sea are ice free for part of the year and the central Arctic, most of the Beaufort Sea and the CAA is ice covered the whole year (Fig. 4a). This pattern is very well reproduced in FESOM, including more ice free days in the Laptev Sea compared to the East Siberian Sea and the retreat of the ice in the Barents and Kara Seas (Fig. 4b).

The intensity of the summer surface PAR is highest in the southernmost areas and decreases towards the pole, with a small tendency towards lower surface PAR closer to Greenland and the CAA, where the ice concentration is highest (Fig. 4c). Despite the northerly location of the Russian shelves and the Chukchi Sea, these areas receive relatively strong average PAR (Fig. 4c) as they are ice free for more than three months during summer (Fig. 4b). Even the areas in the central Arctic that are ice covered the whole year receive some PAR for the most part (Fig. 4c), owing to the sea ice concentration falling below 100% during summer (Fig. 3).

3.2. Dissolved inorganic nitrogen

In REcoM2, the mean surface DIN concentration is highest in the Chukchi and Nordic Seas where DIN is supplied from the North Pacific and Atlantic Oceans (Fig. 5a) as is also the case in WOA13 (Fig. 5b). The largest difference is that the modeled mean concentration in the Nordic Seas is somewhat low compared to WOA13. The Nordic Seas and the Chukchi Sea are nevertheless subject to large seasonal variability in DIN concentrations. During winter when productivity is limited by light availability, DIN is resupplied to the surface mixed layer by e.g. deep mixing. As light limitation is alleviated, the surface DIN is exhausted in all areas except for the central Arctic where the ice is thickest, and phytoplankton growth is light limited (Fig. 5c and d). In the model, the advective transport through the Fram Strait and the Barents Sea Opening increases the surface DIN concentration in the Barents Sea and north-east of the Fram Strait. Some DIN is further transported northwards from the Barents Sea through the St. Anna Trough to meet the Atlantic water from the Fram Strait, thereby supplying DIN to the central Arctic. Nutrient rich water likewise flows from the Bering Strait along the edge of the Beaufort Gyre towards the CAA. In the central Beaufort Gyre, where downwelling dominates, the surface DIN concentration in REcoM2 is thus relatively low. The few measurements from the central Arctic in WOA13 indicate that the low modeled DIN concentration is realistic (Fig. 5a and b). The fact that DIN is not depleted in the Eurasian Basin during summer also fits well with observations showing that nutrient concentrations stay above limiting values at least until August in the Makarov and Nansen Basin (Olli et al., 2007; Boetius et al., 2013), though it may be depleted later in the year.

The modeled DIN concentration is low on the Russian shelves and especially in the East Siberian Sea, with the exception of the coastal areas close to major river mouths, such as the Lena Delta in the Laptev Sea, where nutrients are added to the water through riverine supply (Fig. 5a). This is in good agreement with the WOA13 average (Fig. 5b). During winter, when uptake of nutrients by phytoplankton stops due to light limitation, the DIN concentration increases in the Laptev Sea (Fig. 5c) as nutrients are continuously supplied from the Lena River. The nutrients from the Laptev Sea are advected in the transpolar drift, and thus supply nutrients to the central Arctic surface water (Fig. A.15).

3.3. Dissolved inorganic silicon

The mean surface concentration of dissolved inorganic silicon (DSi) in the model is characterized by high concentrations on shelves close to the major river mouths, especially in the Laptev and Kara Seas, with the concentration falling rapidly towards the open ocean to average concentrations lower than 5 mmol Si m^{-3} (Fig. 6a). In the Chukchi Sea, the DSi concentration is elevated compared to the central Arctic, while the mean concentration in the Greenland and Barents Seas as well as in the

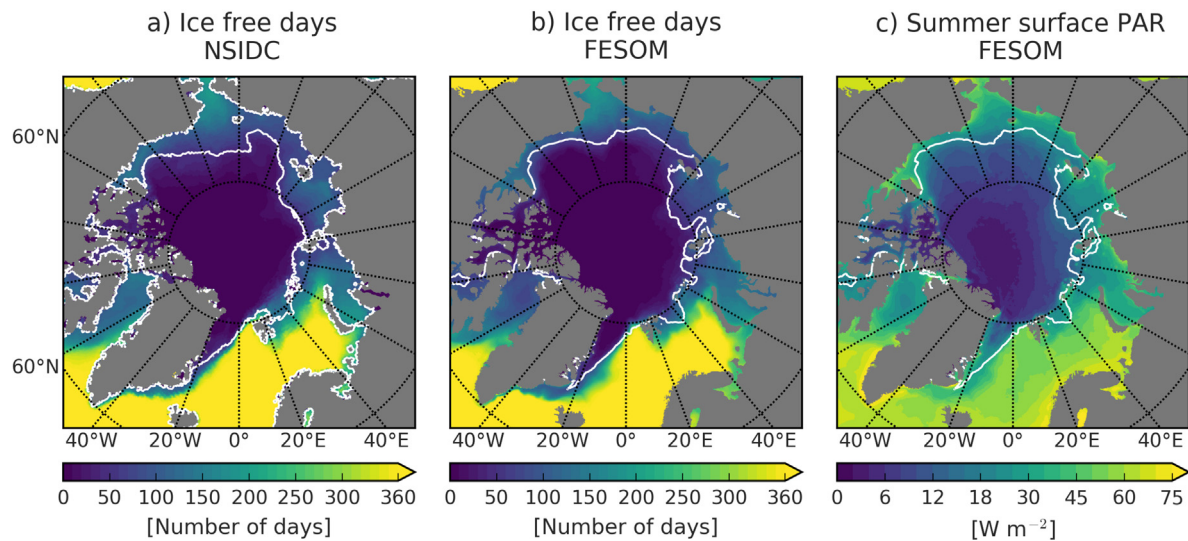


Fig. 4. Average number of yearly ice free days, defined as an ice concentration lower than 10%. The white line marks the average 10% ice concentration for September. (a) Calculated from NSIDC's satellite-based data (Cavaliere et al., 1996) and (b) in FESOM. (c) The mean value of surface PAR during summer (May to September) in FESOM, notice the nonlinear color scale.

central Arctic is relatively low (Fig. 6a).

The imprint of the DSI-rich Pacific water is clear in the Chukchi Sea of WOA13 (Fig. 6b), while the concentration is less elevated in this area in the model (Fig. 6a), though concentrations increase during winter (Fig. 6c). The volume transport through the Bering Strait is well reproduced in FESOM (not shown), but the surface DSI concentration in the North Pacific (60 to 66°N) is on average $15 \text{ mmol Si m}^{-3}$ lower than the values in WOA13. The average input of DSI through the Bering Strait is 3.5 kmol s^{-1} , substantially less than the 21 kmol s^{-1} found by Torres-Valdés et al. (2013), and it makes up half of the amount supplied by riverine DSI to the Arctic in the model (7.6 kmol s^{-1}). One reason for the low concentration of DSI in the modeled North Pacific is a relatively strong degree of iron limitation in the area; the variable stoichiometry in REcoM2 has the consequence that when diatoms are iron-stressed the intracellular ratio between silicon and nitrogen increases, with the result that higher ratio of silicon than nitrogen is exported out of the surface layer. Overall, the model's pattern of highest DSI concentrations on the Arctic shelves and north of Greenland and the CAA fits well with WOA13, but the model's surface DSI concentration is lower than that in WOA13. Further, DSI is thought to decrease from the Bering Strait, across the central Arctic and towards the Nansen Basin (e.g. Gosselin et al., 1997; Varela et al., 2013), something that is somewhat reproduced in the model for the maximum DSI concentration, but cannot be seen during summer, most likely due to the too small inflow through the Bering Strait.

The total riverine input of DSI to the Arctic Ocean in the model is 7.6 kmol s^{-1} , less than the $12.87 \text{ kmol s}^{-1}$ estimated by Torres-Valdés et al. (2013). Despite of this, the DSI concentration in the vicinity of river mouths is higher in the model compared to WOA13 (Fig. 6b). Additionally, we have a relatively strong off-shore gradient of the DSI concentration northwards from the river mouths in the model. Something that has also been documented in observational studies, which show that concentrations generally are elevated in the vicinity of the river mouth but fall rapidly towards the open ocean, for example in the Laptev (Létolle et al., 1993) and the Beaufort Seas (Tremblay et al., 2014). The impact of isopycnal diffusion on the spreading of the riverine DSI will further be discussed in Section 4.6.

In summary, the riverine inflow of DSI has a large influence on the Arctic surface DSI in the model, while the inflow from the Bering Strait is too small. The latter especially affects the DSI distribution in the Canada Basin.

3.4. Limitation of production

The nutrient uptake limitation in the model follows the Michaelis-Menten formula, while the light limitation is defined as the C-specific photosynthesis rate divided by the maximum photosynthetic rate as described in the Appendix (Section 7, Eqs. (A.1) and (A.2)). The limitation factors have values between 0 and 1 at a given time and place, and we define a factor to be limiting when it drops below 0.5. For the nutrient limitation terms this means that a nutrient will be counted as limiting when the water's nutrient concentration is equal to, or less than, the half saturation constant of the phytoplankton. Due to the non-linearity of the limitation factors, they are calculated for every saved output (every second day) and subsequently averaged over the summer period (May to September, Eq. (A.4), Appendix). From this average, the most limiting nutrients for the Arctic summer have been plotted (Fig. 7). Note, however, that the limitation regime varies significantly with time of the year and depth, as will be discussed below.

Light availability is low for much of the year in the Arctic Ocean due to low angle of the incoming radiation combined with extensive ice cover. This leads to light being the main limitation factor for nanophytoplankton in ice covered areas of the model (Fig. 8a). In the coastal areas, where ice breaks up during the summer, light limitation is briefly alleviated. Outside of the average summer ice extent, DIN is the main limiting factor for nanophytoplankton (Fig. 7a), though less in the Norwegian Sea (Fig. 8c) where nutrient rich water is advected northwards from the North Atlantic. The incoming irradiance is, however, still low enough to also be limiting for part of the summer in the ice free areas (Fig. 8a).

In REcoM2, diatoms have a larger initial slope of the photosynthesis-irradiance curve than the nanophytoplankton, leading to diatoms being less sensitive to light limitation (Fig. 7b). Diatoms consequently have a larger potential for productivity in low-irradiance areas, such as underneath the ice and deeper in the water column, as long as nutrients are available. This also means that they dominate in the initial spring bloom. Additionally, light does not limit diatom productivity for long during summer in the ice free areas of the Greenland and Barents Seas (Fig. 8b). In REcoM2, silicon is the main limiting nutrient in almost the whole Arctic Ocean for diatoms, except for the riverine influenced areas in the Kara and Laptev Seas (Figs. 7b and 8e) where the rivers supply DSI to the water. On the Russian shelves, the high DSI to DIN ratio of the riverine input means that phytoplankton growth can only partly use up the DSI supplied due to nitrate limitation. This in turn leads to a

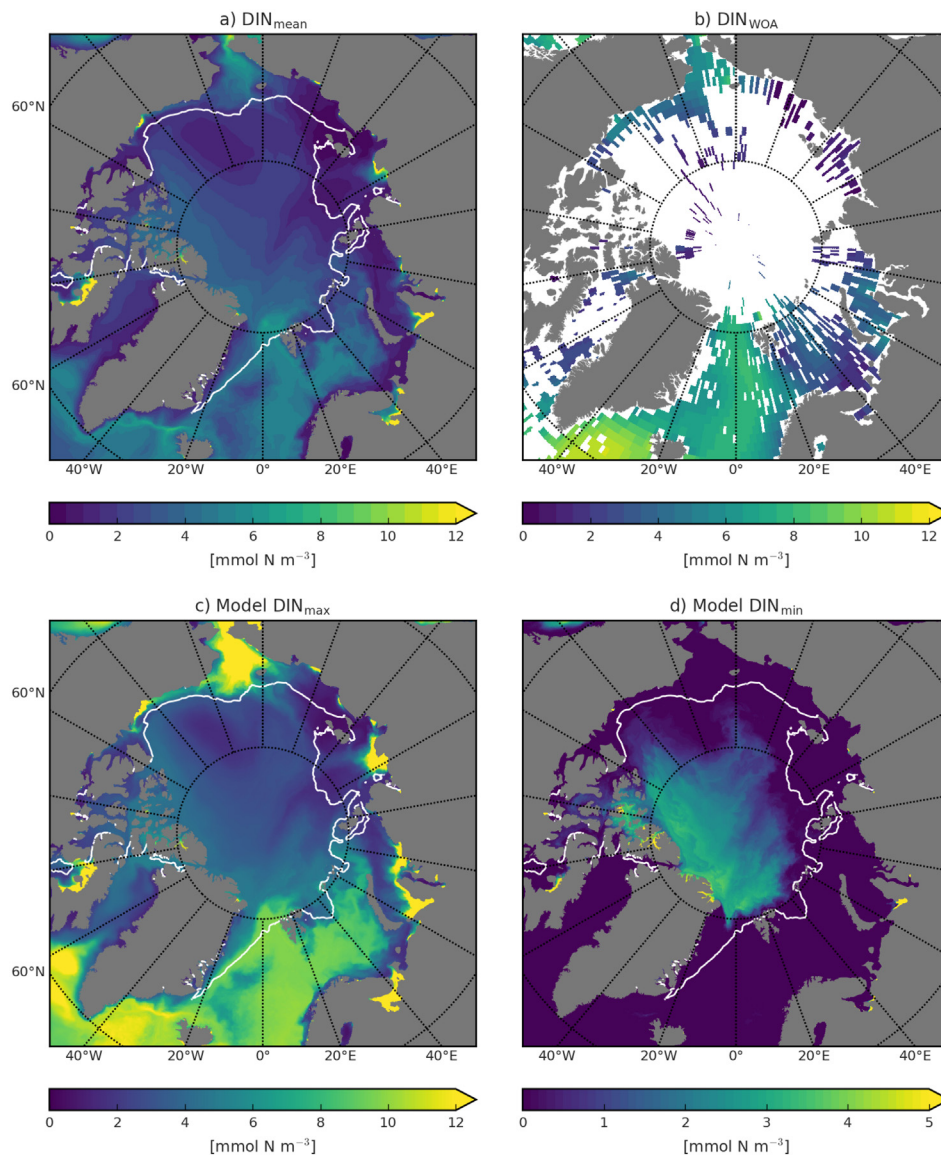


Fig. 5. (a) Modeled mean surface DIN concentration for 2011 to 2015. (b) Mean surface DIN concentration in World Ocean Atlas 2013 (Garcia et al., 2014), for which areas without measurements have been masked out. (c) Modeled maximum surface DIN concentration. (d) Modeled minimum DIN concentration. The white line marks the average 10% ice concentration for September.

stronger N-limitation close to the river mouths (Fig. 7b), as was also found by Le Fouest et al. (2013). A number of studies show that while DIN limitation dominates in the Canada Basin during summer, DSI may be more limiting in the Eurasian basin for diatoms (e.g. Codispoti et al., 2013; Fernández-Méndez et al., 2015). In our setup, we also have DSI limitation in the Canada Basin, probably because of the model's relatively low concentration of DSI in the North Pacific, which leads to a low import through the Bering Strait (See Section 3.3).

The strong seasonality in the Arctic Ocean means that the limitation regime changes significantly with time and depth. Early in the year light limits production in the whole Arctic for both phytoplankton groups, though less so for diatoms (Fig. 8a and c). As the season progresses and biological production takes up nutrients, the nutrient concentration falls, and nutrient limitation sets in. Deeper down in the water column, light limitation is stronger than in the surface due to the attenuation coefficient of the water, while nutrient concentrations increase with depth.

3.5. Productivity

3.5.1. Surface chlorophyll *a*

The modeled mean summer surface chlorophyll (Fig. 9a) has the highest concentrations in the inflow regions of the Greenland, Barents and Chukchi Seas, while they are significantly lower in the central Arctic, except for the areas close to river mouths (Fig. 9a). The higher mean concentrations in the eastern Greenland Sea can mainly be attributed to the earlier onset of the bloom in this area (Fig. 10 and A.14a); the high irradiance compared to the irradiance in ice covered areas and continued supply of nutrients from the North Atlantic means that light and nutrients are readily available, allowing for the bloom to start in April, with surface production continuing until early October as can be seen in the animation of the development of the surface chlorophyll *a* (Fig. 10). In comparison, the more persistent ice cover, and associated stronger light limitation, in the Chukchi Sea (Fig. 8a and c) means that the bloom begins a month later here despite the high nutrient availability early in the year. On the Russian shelves, the growth season is relatively short, firstly due to ice coverage and secondly due to low DIN availability away from the river mouths (Fig. 5a). The highest

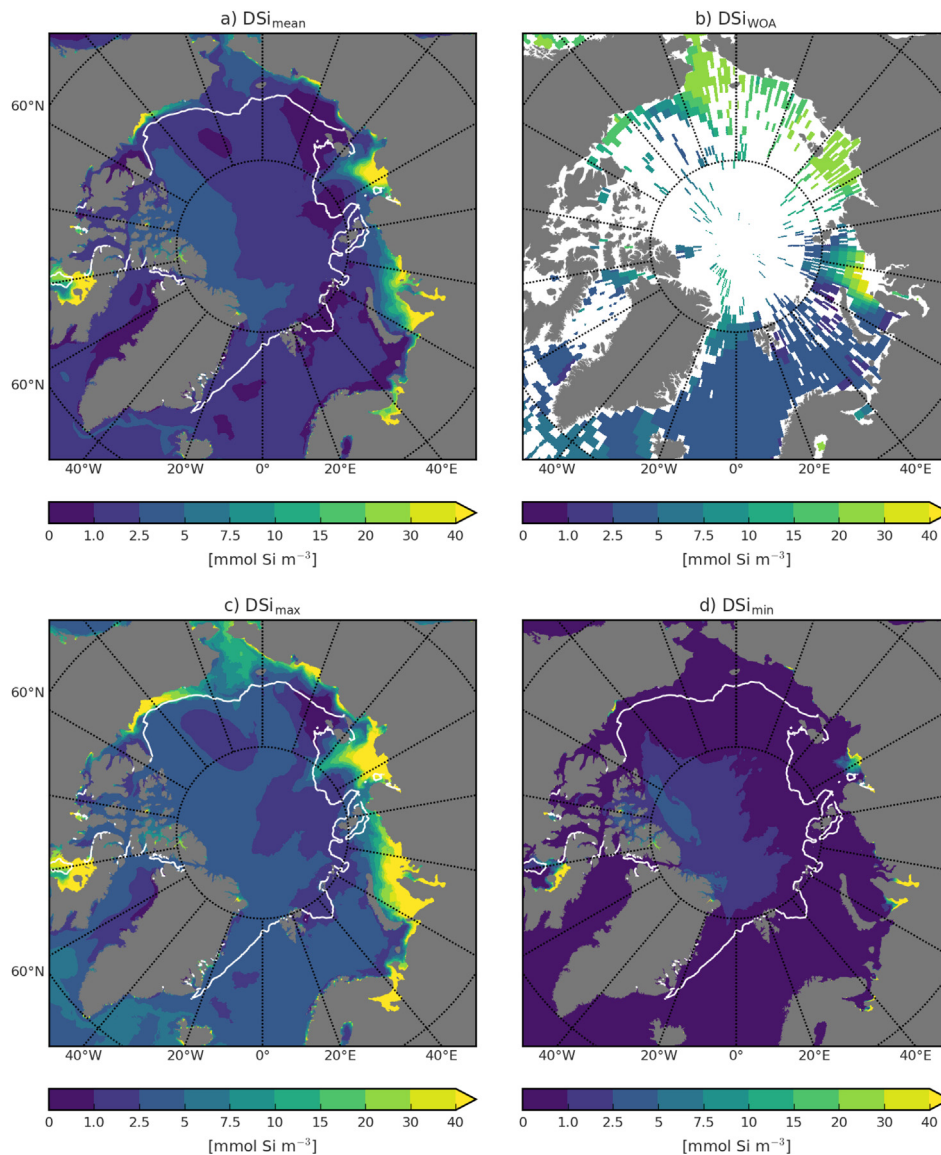


Fig. 6. (a) Modeled mean surface DSi concentration for 2011 to 2015. (b) Mean surface DSi concentration in World Ocean Atlas 2013 (Garcia et al., 2014). Points without measurements have been masked out. (c) Modeled maximum surface DSi concentration. (d) Modeled minimum DSi concentration. Notice the nonlinear colorbar. The white line marks the average 10% ice concentration for September. (For interpretation of the references to colour in this figure legend, the reader is referred to the web version of this article.)

concentrations of chlorophyll *a* are thus located around the major river mouths, where the ice breaks up relatively early and nutrients are continuously supplied from the rivers (Fig. 9a). The model has rather pronounced ice edge blooms throughout the year, starting as light limitation is alleviated by the retreating sea ice. As the season progresses and the incoming radiation increases at the same time as the melting reduces the sea ice concentration, more light becomes available below the sea ice, and the front edge of the bloom moves further in under the ice in some areas. In 2015, this mainly took place in the Canada Basin (Figs. 3 and 13), but this changes dependent on ice conditions of the year in question.

Overall, the spatial distribution is very similar in the modeled surface chlorophyll and the satellite-based estimate, with the exception of the Russian shelves (Fig. 9). In the Greenland Sea, both chlorophyll fields have a tongue of high chlorophyll concentration in the Norwegian Atlantic Current where the nutrients are brought in from the North Atlantic, and where the bloom starts first. A second tongue can be seen along the ice edge east of Greenland, where the melt water stabilizes the water column early in spring, though it is less pronounced in the

model where the bloom moves downwards in the water column as the season progresses (Fig. 10). In the Barents Sea, the two chlorophyll fields are also very similar, with high chlorophyll concentration towards the south and lower towards the north. The southern Barents Sea is ice free for the whole year, and like the eastern Greenland Sea, the modeled growth starts early here in late April, and continues throughout the summer as nutrients are mixed into the surface layer. In the northern Barents Sea the bloom follows the ice edge northwards as it retreats, and the growth season is thus shorter. The Canada Basin is characterized by having an extensive ice cover most of the year, and the chlorophyll concentration is therefore highest in coastal regions, where nutrients are supplied by rivers and the ice breaks up earliest, and in particular in the Chukchi Sea where nutrients are supplied from the Pacific. In the Chukchi Sea, a lot of the difference in magnitude between the two chlorophyll fields can be explained by the timing of the bloom; the satellite-based estimates only contain values from open water, while the bloom in the model has increased chlorophyll values below the ice from May onwards (Fig. 10 and A.14). But another issue is the relatively low input of DSi from the North Pacific to the Arctic Ocean through the

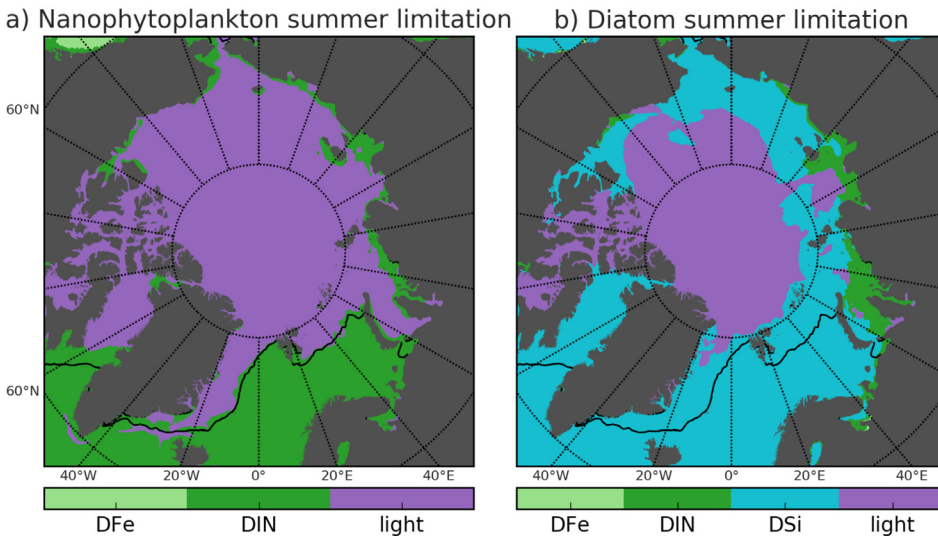


Fig. 7. (a) The most limiting factor for surface nanophytoplankton from May to September. (b) The most limiting factor for surface diatoms from May to September. The black lines show where the average summer (May to September) ice concentration is 10%. DFe: Dissolved Iron, DIN: Dissolved inorganic nitrogen, DSi: Dissolved inorganic silicon.

Bering Strait; this means that the diatom class in the model is more silicon limited than it would be with a larger DSi input.

When comparing our modeled surface chlorophyll with the satellite-based estimates of chlorophyll *a*, it is, however, clear that the satellite-based values are generally higher than the modeled, especially on the Russian shelves (Fig. 9). Some possible explanations are the following: Firstly, in the model results we take the value at each time step and each location into account when calculating the summer mean, while the satellite-based estimate has much fewer available data points. This mainly introduces a bias in the areas that are ice covered or dark for part of the year, as the satellite-based mean is calculated from a very short period of open water in which productivity is relatively high. Secondly, the concentration of colored dissolved organic matter

(CDOM) is high on the Russian shelves, introducing a positive bias in the satellite-based estimates in this region (e.g. Matsuoka et al., 2007).

It is, however, likely that the modeled surface chlorophyll concentration is on the low side in the Greenland Sea. Here, the modeled pre-bloom nutrient concentration is low compared to observations (Section 3.2), meaning that the potential for productivity is also lower. Additionally, despite the high resolution, we do not capture the small scale disturbances that help resupply the nutrients from below to the full degree.

The high horizontal resolution has a pronounced effect on the spatial distribution of chlorophyll during the spring bloom (Fig. 10). This is especially noticeable in the Nordic Seas where the model resolution is high compared to the Rossby radius of deformation (Nurser and Bacon,

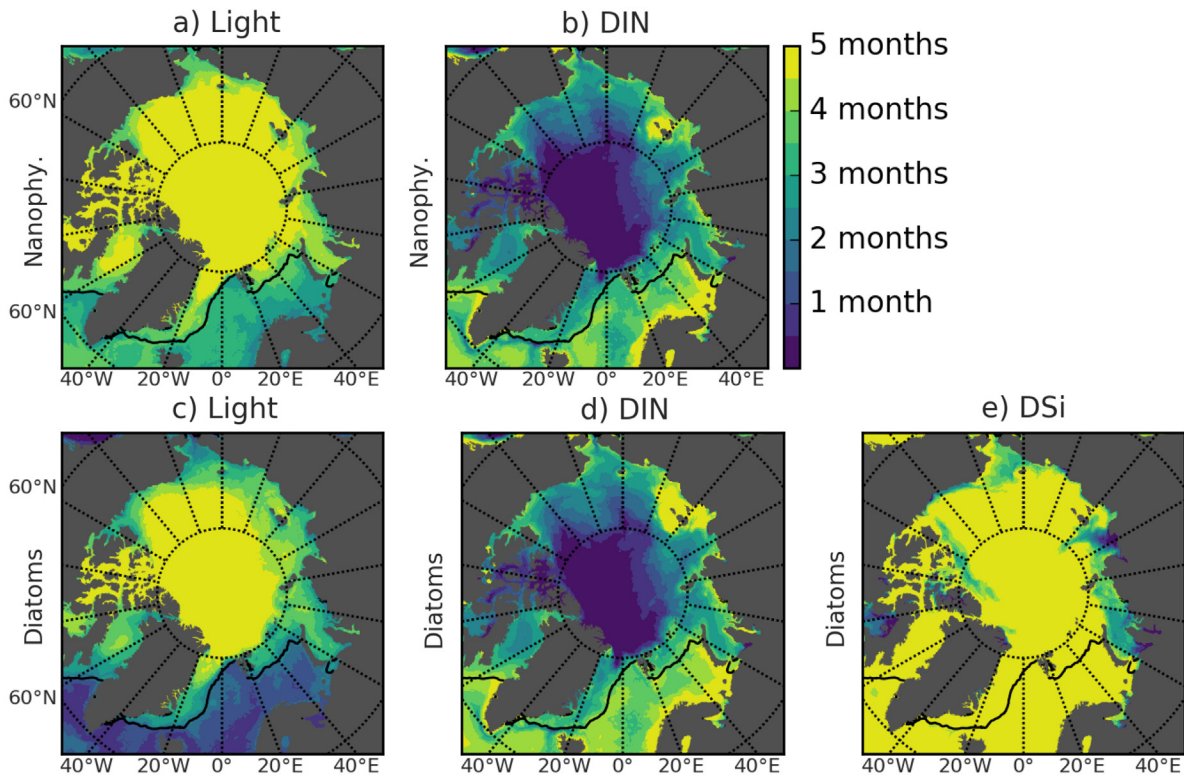


Fig. 8. The time period in which the different limitation factors are smaller than 0.5. (a) Light for nanophytoplankton. (b) DIN for nanophytoplankton. (c) Light for diatoms. (d) DIN for diatoms. (e) DSi for diatoms. The black lines show where the average summer ice concentration is 10%.

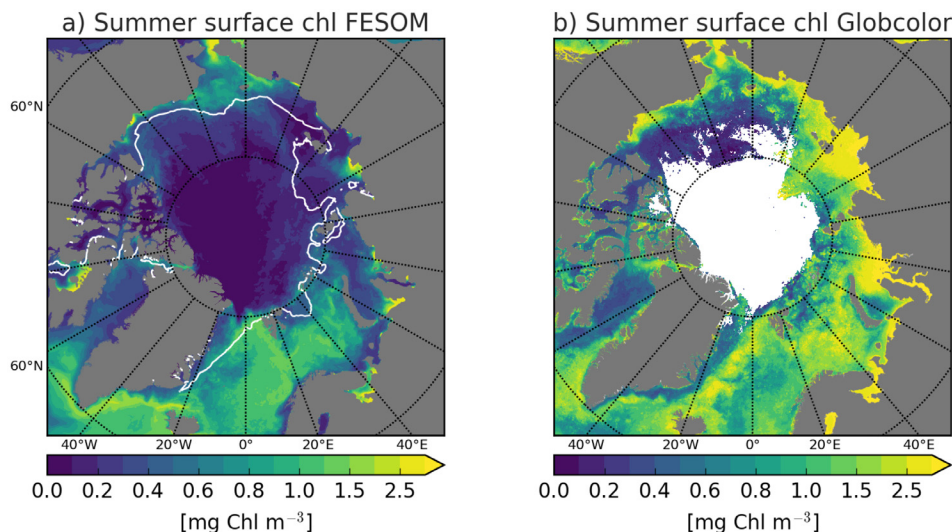


Fig. 9. (a) Summer mean (May to September) of modeled surface chlorophyll *a* concentration. The white line marks the average 10% ice concentration for September. (b) The summer mean surface chlorophyll *a* concentration from Globcolor (www.globcolor.info).

2014), leading to the surface chlorophyll being characterized by an eddying and meandering pattern that is not seen in coarser model runs. In the Barents Sea, the presence of a strong Arctic Front means that the bloom can develop in the frontal area earlier than in the rest of Barents Sea open water, as has also been observed in satellite-based studies (e.g. Oziel et al., 2017). In ice covered areas the resolution means that isolated blooms develop independently below the ice. Once the surface nutrients have been depleted in the Nordic Seas, the resupply of nutrients is highly correlated with negative vorticity in the model (not shown). For the surface chlorophyll, this is especially clear in September, when an eddying pattern is clearly visible (Fig. 10).

3.5.2. Subsurface chlorophyll maxima

Here, we follow Steiner et al. (2016) and define the SCM to occur when the chlorophyll *a* maximum is located below the surface at a given time and space. Following this definition, SCMs occur to some degree in the whole Arctic Ocean in the model, with the exception of the central Arctic where growth is strongly light limited (Fig. 11a). In general, the modeled bloom starts near the surface, where light and nutrients are readily available in the beginning of the season. When the pool of surface nutrients is exhausted, the production follows the nutricline downwards in the water column, provided that the light level at the depth of the nutricline is sufficient to support growth. The low minimum surface nutrient concentrations in the model also give an

indication of where the surface nutrients become exhausted and growth only can take place deeper in the water column (Figs. 5d and 6d). The duration of the SCM ranges from less than two weeks in permanently ice covered areas, to 4.5 months along the Norwegian coast (Fig. 11b). In general, the duration of the SCM is longest in the Greenland and Barents Seas, where the growth season is longest and the intensity of the incoming light is high enough to support a SCM. On the Arctic shelves and in the Chukchi Sea, the SCM lasts less than three months, reflecting the fact that the ice is present for a longer time here, thereby shortening the growth season. The fact that the mean depth of the SCM reflects its duration (Fig. 11b and c), is explained by the nutricline moving deeper into the water column with time, thereby also moving the SCM downwards. In REcoM2, the C:Chl ratio is variable, and the algae can photoacclimate to a lower irradiance regime by decreasing the C:Chl ratio as also happens in the ocean. It is thus possible that REcoM2 predicts more widespread SCMs than what is the case in models with fixed C:Chl ratios.

Along the ice edge, the SCM occurs at relatively shallow depths throughout the Arctic (Fig. 11c). The melting of sea ice stabilizes the water column, thereby also stabilizing the nutricline. Additionally, light limitation is stronger here, thereby limiting the depths to which a SCM can develop.

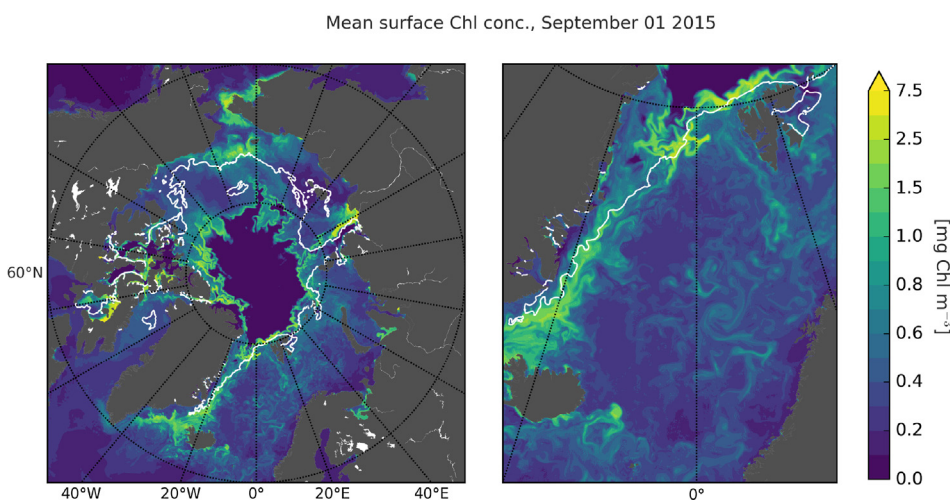


Fig. 10. Placeholder for the animation “FESOM-REcoM2_Ch12015.mp4” submitted as supplementary material: An animation of the spatial distribution of the modeled surface chlorophyll *a* concentration for the year 2015. The plot to the right is a zoom of the Nordic Seas, which is the area with the highest resolution relative to the Rossby radius of deformation, and thus the area with the most eddy activity. The white line marks the 10% ice concentration contour.

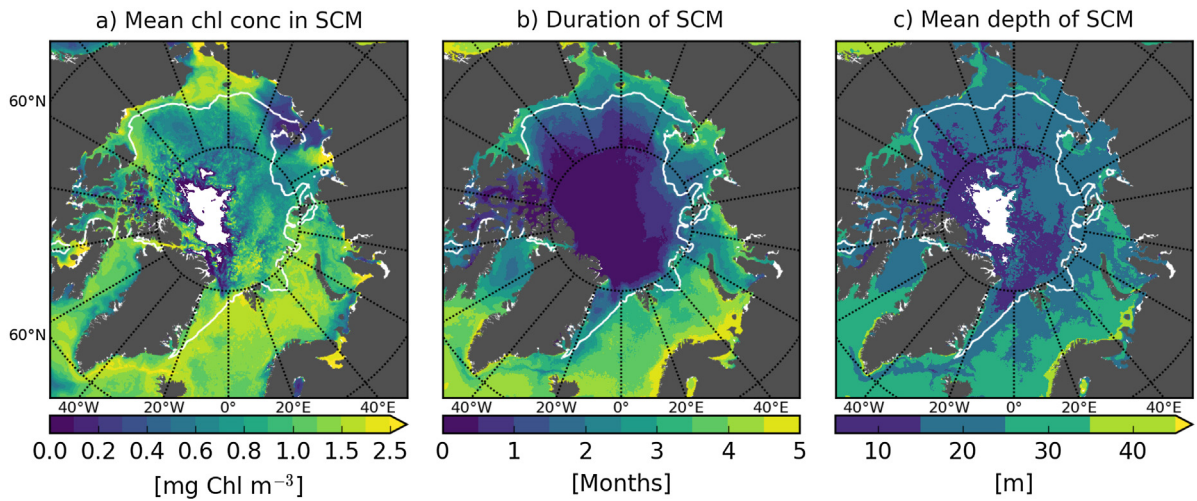


Fig. 11. (a) Mean chlorophyll *a* concentration in the SCM, calculated for the period in which a SCM is present. (b) The time period a SCM is present. (c) Mean depth of the SCM calculated for the time period in which a SCM is present. The white line marks the 10% September sea ice concentration.

3.5.3. Primary productivity

For the AO, the average yearly NPP from 2011 to 2015 is 445 Tg C yr⁻¹ in the model (Fig. 12a), with 70% of the total NPP being from diatoms. Approximately a third of productivity is associated with the pelagic, the ice free shelf and the ice zone, respectively. Most of the production (43%) takes place in the pelagic zone (Definition in Section 2.4), which is mainly located in the Greenland and Barents Seas, as the other zones tend to be shallow or ice covered for most of the year (e.g. Fig. 1b). High average rates occur in the Norwegian Atlantic Current (Fig. 12b), which runs northward along the coast of Norway, then separates in two branches, one continuing towards Svalbard and one branching off into the Barents Sea. This pattern is similar to that of surface chlorophyll concentration, and can be explained by the northward transport of nutrients within the Norwegian Atlantic Current, and by the upward mixing of nutrients due to the strong current combined with relatively high light availability, leading to a long growth season here.

On average, 25% of all productivity takes place on the ice free shelves (Fig. 12a), most of it in the Barents and Chukchi Seas (Fig. 12b) where nutrients are readily available and the ice retreats relatively

early. On the Russian and Beaufort Sea shelves, most productivity takes place along the coast, especially downstream of riverine nutrient input.

A similar fraction of the production (32%) is associated with the ice zone, with the production in the marginal ice zone making up a bit less than the under ice production (12 vs. 20%). Ice edge blooms, which are in the MIZ category here, mainly occur as the ice retreats (Fig. 13) and the water column stabilizes, while the nutrient concentration is still high in the surface water. In areas where the ice concentration falls in summer, the front of the bloom moves further in below the ice, while separate blooms also form under the ice. Later in the year, when the surface nutrients are becoming depleted, the highest rates of the under-ice productivity can be found at the front of the bloom below the ice, while the low nutrient availability lead to lower productivity in the majority of the Arctic Ocean (Fig. 13). Under-ice productivity takes place in both the Canadian and Eurasian Basin in areas where the ice concentration is low enough to let light through.

In the satellite-based estimate of Arctic NPP (Fig. 12c), the productivity is very uniform at about 300 to 450 mg C m⁻² day⁻¹ across most of the Arctic Ocean. This is fairly similar to the modeled rates in the Greenland, Barents and Chukchi Seas (Fig. 12b and c). On the

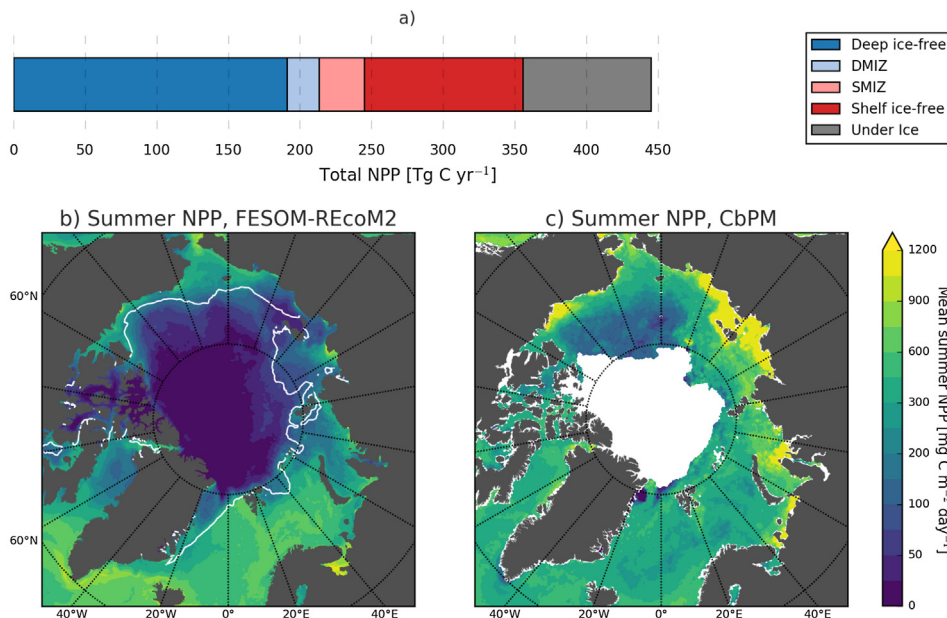


Fig. 12. (a) Total NPP in the different ecological zones following (Pabi et al., 2008, their Fig. 9). (b) Average modeled summer NPP (May to September). The white line marks the 10% September sea ice concentration. (c) Average summer NPP from the CbPM satellite-based estimates (<http://orca.science.oregonstate.edu/2160.by.4320.8day.hdf.cbpm2.m.php>).

Mean NPP, September 01 2015

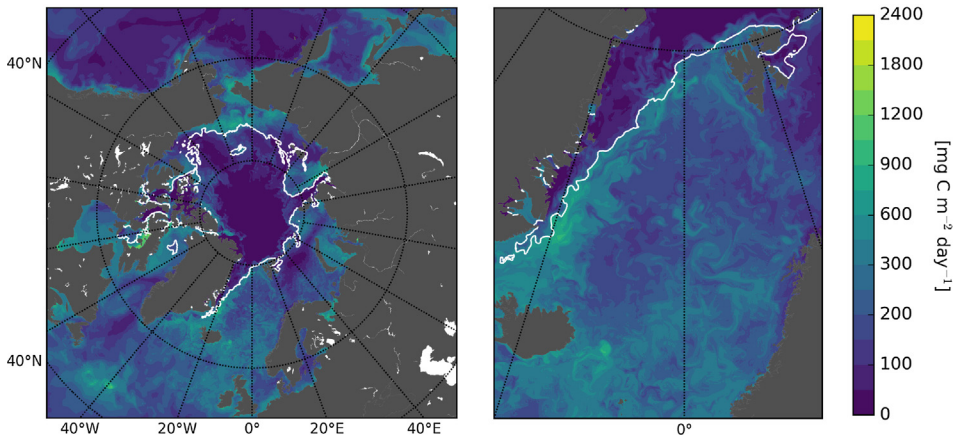


Fig. 13. Placeholder for the animation “FESOM-REcoM2_NPP2015.mp4” submitted as supplementary material: The animation shows the spatial distribution of the modeled vertically integrated net primary productivity for the year 2015 based on bi-daily model output. The plot to the right is a zoom of the Nordic Seas, which is the area with the highest resolution relative to the Rossby radius of deformation, and thus the area with the most eddy activity. The white line marks the 10% ice concentration contour.

Russian shelves, however, the NPP is significantly higher than in the rest of the Arctic Ocean in the satellite-based estimates, while our modeled mean NPP is relatively low on the Russian shelves. In both models, hot spots of productivity are located around the mouths of the major rivers (Fig. 12a), areas characterized by having a relatively high supply of nutrients from the rivers. But the effect of the rivers seems much larger in the satellite-based estimates than in REcoM2. As is the case for surface chlorophyll, the difference can possibly be attributed to known challenges for the satellite-based estimates on the shelves (Section 2.5), but also the underestimation of mixing on the shelves may attribute to this. As the satellites can not measure under ice, the under-ice productivity can not be compared.

4. Discussion

4.1. Modeled versus observed nitrate

FESOM-REcoM2 captures the DIN gradient across the Arctic Ocean, with high concentrations in the inflow regions and lower concentration in the central basins as illustrated by e.g. WOA13 (Fig. 5a and b). WOA13 is, however, based on sparse measurements, especially in the central Arctic and we therefore now discuss our results in relation to more local studies. Codispoti et al. (2013) presented seasonally collected nutrient measurements, which confirm that the modeled Chukchi Sea pre-bloom and summer DIN concentration are realistic (their Fig. 4a and b). In the central Arctic, surface DIN concentrations have been shown to be relatively low, especially in the Canada Basin, where Codispoti et al. (2013) showed that the pre-bloom surface DIN concentrations were close to zero, and even in coastal regions, winter re-supply is small (Tremblay et al., 2008). This pattern fits well with the distribution we find in FESOM-REcoM2, with low DIN concentrations in the Beaufort Gyre and higher concentrations towards the central Arctic under the ice (Fig. 5). The modeled post bloom nutrient limitation in the Beaufort Sea also agrees with observations (Tremblay et al., 2008; Taylor et al., 2013b). In the Nansen basin, which receives nutrients from the North Atlantic, Packard and Codispoti (2007) measured pre-bloom values of 4 mmol N m^{-3} below the pack ice as we also see in the modeled pre-bloom DIN concentration, while Fernández-Méndez et al. (2015) reported post-bloom values smaller than 1 mmol N m^{-3} both at the Laptev Sea margin and at in the central Arctic, supporting our findings of relatively low post-bloom nutrient concentrations, and thus nutrient limitation, in areas of low ice coverage in the central Arctic.

The pre-bloom DIN concentration of 10 to 11 mmol N m^{-3} found by Reigstad et al. (2002) in the central Barents Sea is well reproduced in our run. In the Nordic Seas, however, FESOM-REcoM2 produces a complete drawdown of surface nutrients in summer (Figs. 5d and 6d), while measured summer DIN concentrations tend to be higher in the

area ($0\text{--}5 \text{ mmol N m}^{-3}$, Codispoti et al., 2013). Part of the reason is that we show the minimum concentration, while their database spans the time period from June to October, meaning that autumn storms may have brought nutrients from deeper reservoirs to the surface. This is supported by the fact that the modeled mean surface DIN concentration in the Greenland Sea (65 N to 80 N and -45 W to 15 E) increases from $1.5 \text{ mmol N m}^{-3}$ on the 1st of October to 4 mmol N m^{-3} on the 30th of October. Also the formulation of zooplankton in the model has an effect on the surface nutrients; currently, our one zooplankton class predominantly grazes on the nanophytoplankton class in the model, leading to a large uptake of DIN by diatoms in the spring. Stronger grazing pressure on the diatoms class would change the nutrient retention in the surface water, both by decreasing the uptake by phytoplankton and also by direct release of DIN during the grazing process. An interesting feature is the clear impact of eddies in the Nordic Seas towards the end of the growth season; in September, upwelling associated with anticyclonic eddies brings nutrients to the surface water, thereby also increasing the surface productivity.

4.2. Subsurface chlorophyll maxima

In recent years, SCMs have been observed in many areas of the Arctic Ocean (e.g. Erga et al., 2014; Martin et al., 2012), but their distribution and duration are not well constrained by measurements. SCMs are thought to occur in the transition zone where the nutricline and euphotic zone overlap when the nutrient concentration above the nutricline becomes too low to support growth (e.g. Cullen, 2015). As our simulated surface DIN and DSi becomes depleted during summer in the whole ice free area of the Arctic Ocean (Fig. 5d and 6d), production moves below the surface during the time when the incoming radiation is strong enough to support growth deeper in the water column (Fig. 11b). This widespread occurrence of SCMs is a feature that FESOM-REcoM2 shares with a number of other models (Popova et al., 2010; Steiner et al., 2016). In a model intercomparison study for the Canada Basin, Steiner et al. (2016) showed that SCMs occur in models with a reasonably low surface DIN distribution. In our study, the average depth of the SCM varies from 10 to 30 meters in most regions, including the Canada Basin (Fig. 11c). This fits well with the models analyzed by Steiner et al. (2016), while their measured SCM (McLaughlin and Carmack, 2010) occurs deeper in the water column (60 m for 2011 to 2014), possibly due to a slightly shallow bias in our modeled mixed layer depth (MLD, not shown). However, Brown et al. (2015) showed that the depth of the SCM varies significantly for the Chukchi shelf. From a large database of chlorophyll profiles in the Greenland Sea, Cherkasheva et al. (2013) showed that the SCM on average is strong in July and August, while the duration of the SCM in the Fram Strait was more variable. In our model run, the SCM in the

Greenland Sea is present for a longer period (Fig. 11b), while the situation in the Fram Strait is variable between the years, dependent on the location of the ice edge. In the Barents Sea, a SCM has been observed in early June at a depth of 40 meters, while it was located at 30 meters in July (Vernet, 1991). These observations show that the SCM indeed develops early in the Barents Sea, as is also the case in FESOM-REcoM2, though Vernet (1991) mentions that location of the SCM is dependent on the location of the Polar Front in the Barents Sea. On the outer shelf of the Laptev Sea, a September SCM was observed by Heiskanen and Review (1996) at 30 meters of depth, while we have a SCM at 20 m in the area (Fig. 11a). At this stage, we can say that a modeled wide spread SCM in the Arctic is realistic, but the detailed assessment is beyond the scope of this study.

4.3. Integrated Arctic primary production

Our pan-Arctic NPP estimate of 445 Tg C yr^{-1} (Fig. 12a) is in the middle of the range of other estimates ranging from 329 Tg C yr^{-1} (Sakshaug, 2004) to $626 \pm 20 \text{ Tg C yr}^{-1}$ (Popova et al., 2010). Relatively high estimates are given by Popova et al. (2010) and Arrigo and van Dijken (2015), who look into the years 1990 to 2006 and 1998 to 2012, respectively. Popova et al. (2010) are using an OGCBM, which is similar in complexity to our model, but on a coarser grid. The high NPP rates from the satellite-based estimates presented by Arrigo and van Dijken (2015) is largely explained by the high rates of NPP on the Russian shelves, which we do not have in our run, while the open ocean productivity rates are similar to those in our model run. The low value of 329 Tg C yr^{-1} from Sakshaug (2004) was, on the other hand, based on a compilation of early measurements and model runs, and the lower result therefore may reflect a more ice-covered and less productive Arctic as compared to more recent estimates. A number of other studies have values of integrated pan-Arctic NPP that are close to ours (e.g. Jin et al., 2012; Pabi et al., 2008). One caveat in our model run is the low inflow of DSI from the North Pacific to the Chukchi Sea, which may mean that our modeled NPP is lower than it could be if the DSI supply was higher. A larger supply of DSI would, however, only increase the diatom production until DIN becomes limiting. As the surface DIN concentration is already low during summer in the Chukchi Sea (Fig. 5d), this means that a higher DSI inflow would likely not have a large effect.

In the following we will look closer at the production in the ice zone and on the Russian shelves, which are areas where the largest differences between different studies can be found.

4.4. Ice zone productivity

The modeled productivity in the ice zone is the most difficult to assess, as this zone covers a large and inaccessible area with few in situ measurements. Traditionally, pan-Arctic estimates of NPP have assumed that the under-ice productivity was negligible due to the strong light attenuation of sea ice and snow (Sakshaug, 2004; Pabi et al., 2008; Arrigo and van Dijken, 2015). But recent studies have shown that under-ice productivity occurs in both the Canadian (e.g. Lowry et al., 2014; Arrigo et al., 2014; Mundy et al., 2009) and the Eurasian basin (Fernández-Méndez et al., 2015). Our study supports the notion of a significant contribution of the under-ice productivity to integrated Arctic NPP (20%, Fig. 12a). This is in agreement with similar model studies, in which the under-ice productivity makes up approximately one third of total productivity (e.g. Jin et al., 2016).

In FESOM-REcoM2, the MIZ blooms especially develop in the Greenland, Barents and Chukchi Seas when the ice recedes (Fig. 13), the water column stabilizes and nutrients are above limiting concentrations. The ice edge blooms, which have also been observed by satellites (Perrette et al., 2011) and *in situ* (e.g. Engelsen et al., 2004; Arrigo et al., 2012), contribute 53 Tg C yr^{-1} to NPP, which is 12% of the Arctic Ocean total production. This is close to the results from the model study by Popova et al. (2010), where it was found that both the SMIZ and

DMIZ contributed 21 Tg C yr^{-1} , respectively, to Arctic NPP, slightly lower than our values. In contrast, Pabi et al. (2008) found that a relatively large fraction, namely 31% (132 Tg C yr^{-1}) of the production occurred in the MIZ, most of it on the shelves. The difference between our results and the satellite-based estimates from Pabi et al. (2008) can be explained by the fact that the total area of the MIZ is almost 3 times smaller in FESOM than in their estimates (0.39 vs. $1.13 \times 10^6 \text{ km}^2$), corresponding closely to the difference in NPP in the MIZ, and showing that the per area productivity is in fact slightly higher in FESOM-REcoM2. The relatively small extent of the MIZ is something we have in common with Popova et al. (2010). While our model setup uses a higher spatial resolution, neither model completely resolves the spatial and temporal heterogeneity of the MIZ and brittleness of the sea ice. Additionally, small scale processes such as turbulence and ice edge upwelling, which contribute to driving the increased productivity in the MIZ (Mundy et al., 2009; Carmack and Chapman, 2003), are not fully captured in the model.

When the intensity of the MIZ bloom declines, production does, however, not necessarily stop, rather, the front of the bloom moves further in below the ice. This development is facilitated by the increasing intensity of radiation in early summer combined with decreasing ice concentration (Fig. 3 and A.14), and contributes significantly to the under-ice productivity. The bloom begins in the ice zone when the ice concentration is around 90% (Fig. A.14), in 2015 this takes place in July in the Canada Basin (Figs. 13 and 3). The ice zone bloom develops at a relatively low strength of surface PAR, in many places it is around 12 W m^{-2} at the time of the onset of the bloom (Fig. A.14c). In comparison, Siegel et al. (2002) found that the compensation radiation for the North Atlantic spring bloom was 32.9 W m^{-2} . One difference between the ice covered Arctic Ocean and the North Atlantic is that the Arctic Ocean is a more stable environment with a stratified water column. This means that less dispersion occurs in the early stages of the phytoplankton growth, thereby allowing the bloom to form. The strength of the surface PAR is not a full explanation for the onset of the bloom; the bloom develops late in a large patch in the Chukchi and East Siberian Seas as compared to surrounding areas, despite of similar ice concentration and light conditions. North of Svalbard the ice starts thinning in early September of 2015, too late for the incident irradiance to drive a bloom below the ice in that particular year.

It has been shown that the under-ice productivity plays an important role in the Arctic (Lowry et al., 2014), a role that will most likely become larger as the Arctic sea ice changes towards a thinner, younger and more fragmented state, with leads and melt ponds further complicating the picture. In FESOM-REcoM, the sea ice fractions into leads, characterized by lower ice concentration than the surrounding ice sheet, especially from June to August (Fig. 3). In the Beaufort Sea, the bloom onset is earlier within these leads (Fig. A.14a), where the strength of PAR is relatively high. This result fits well with observations of earlier bloom onset within leads north of Svalbard (Assmy et al., 2017). Currently, FESOM-REcoM2 uses a relatively simple, but common, parameterization for the amount of light penetrating the ice pack, which does not take the heterogeneity of the ice within a model cell into consideration (Frey et al., 2011; Katlein et al., 2015). Given the strong dependence of the under-ice productivity on the availability of PAR, the model's representation of the productivity here would benefit from an improved light-through-ice parameterization, which also takes the melt ponds into account, as has for example been suggested by Arndt and Nicolaus (2014), and used by Fernández-Méndez et al. (2015).

4.5. Russian shelf productivity

In recent years, the extent of the summer sea ice on the Russian shelves has decreased significantly, leading to renewed interest in the effects on the biology (Arrigo and van Dijken, 2015). The NPP on the Russian shelves of the Kara, Laptev and East Siberian Sea, is, however,

not well constrained; some satellite-based estimates indicate that the rate of NPP is very high and increasing in the area (e.g. Arrigo and van Dijken, 2015) and others show more moderate rates (Pabi et al., 2008; Hill et al., 2013), while large scale OGCBMs differ in their representation of NPP in the area, from very low to relatively high (e.g. Popova et al., 2012). Our results fall in the lower end of the spectrum, with especially low rates of mean summer NPP in the East Siberian Sea and somewhat higher values in the Kara Sea and the coastal Laptev Sea (Fig. 12a). For September, the average modeled NPP in the Kara Sea is $132 \pm 24 \text{ mg C m}^{-2} \text{ day}^{-1}$ and in the Laptev Sea it is $121 \pm 26 \text{ mg C m}^{-2} \text{ day}^{-1}$, with productivity falling towards the end of the month. This relatively low values are supported by measurements of 20 to $359 \text{ mg C m}^{-2} \text{ day}^{-1}$ from the Kara Sea in September (Mosharov, 2010; Vedernikov et al., 1995), while Laptev Sea September measurements showed NPP rates lower than $23 \text{ mg C m}^{-2} \text{ day}^{-1}$ in the open water and moderate values (average 100 to $300 \text{ mg C m}^{-2} \text{ day}^{-1}$) near the Lena outflow (Sorokin and Sorokin, 1996). However, while our result fits fairly well with these measurements, the question is whether it is for the right reason. The low integrated rates of NPP in the Laptev Sea have been suggested to be caused by light limitation brought on by the waters' turbidity (Sorokin and Sorokin, 1996), and the presence of CDOM (Matsuoka et al., 2007). In our model setup, we do not have CDOM incorporated, and the lower productivity is a combination of light limitation, especially off-shore and during sea ice coverage, and nutrient limitation later in the season, especially close to the shore (Fig. 7). Stronger light limitation due to CDOM absorption in the model, and thus less nutrient uptake, could potentially contribute to a larger advection of nutrients from the shelves towards the central Arctic, especially from the Laptev Sea where the transpolar drift branches off towards the north and where the Lena River contributes relatively large amounts of nutrients.

The modeled decrease in NPP from the coastal to offshore areas on the Russian shelves (Fig. 12) is supported by measurements from the Kara and Laptev Sea (Vedernikov et al., 1995; Mosharov, 2010). The highest nutrient concentrations in the measurements occur close to the coast (Mosharov, 2010), indicating that the riverine supply plays an important role on the shelves. Bernard et al. (2011) and Dürr et al. (2011) showed that the riverine DSI input per m^3 of water in the Arctic Ocean is about three times higher than in other world oceans. This indicates that the riverine DSI input indeed plays a large role in the Arctic Ocean and especially on the Arctic shelves as we also see in our model run (Figs. 6 and 7b). Test runs with FESOM-RECO2M2 excluding riverine silicon input, however, shows that the lack of silicon mainly affects the species composition towards more nanophytoplankton rather than the total NPP (not shown), which was also demonstrated by Bernard et al. (2011).

4.6. Choice of resolution

Meso- and submesoscale processes play an important role for ocean mixing, transport of nutrients and heat, and for the depth of the mixed layer (e.g. Spall et al., 2008; Nishino et al., 2011; Bebieva and Timmermans, 2016), especially in the Arctic Ocean, where the Rossby radius of deformation is relatively small and variable (Nurser and Bacon, 2014). It has therefore been repeatedly suggested that increasing the horizontal resolution of a model domain ought to also increase the skill of the model (e.g. Proshutinsky et al., 2011; Deal et al., 2014).

The current work is a first step towards utilizing FESOM's unique multiresolution capabilities in a biogeochemical setup. The choice of an Arctic wide resolution of 4.5 km is a compromise between seeking as high a resolution as possible, and still being able to run the model over a reasonable time period. Our setup is eddy permitting in the Nordic Seas, eddy resolving in the deep central Arctic Ocean, especially in the Canada Basin, and not eddy resolving on the shelves (Wekerle et al., 2017b, their Fig. 2c). In the Nordic Seas, which is a highly dynamical

area, the well defined currents also lead to the spring bloom being highly filamented, thereby recreating the patchiness that characterizes oceanic productivity in reality (e.g. Martin, 2003; Mahadevan, 2016). The imprint of eddies can be seen in the NPP distribution in the Nordic Seas, especially in August and September, when the surface DIN concentration is low and eddy-mediated vertical nutrient transport plays a large role in sustaining productivity (not shown). In the ice covered zone in the central Arctic, the modeled eddy kinetic energy is low (Fig. A.16a) and we do not directly see an effect of resolution on neither nutrient transport (Fig. A.17b) nor productivity. It has, however, previously been shown that the representation of the vertical velocities are improved by resolution as was shown by McKiver et al. (2015) and that the dynamics of the nutrients are changed, for instance by a changed export flux of biomass (e.g. Watanabe et al., 2014). In our run, the vertical eddy mediated transport of DIN is largest in the Nordic Seas and the Barents Sea (Fig. A.17b), while the transport in the central Arctic is dominated by the mean upwelling field, for instance along the shelf breaks (Fig. A.17a).

In FESOM, we apply Redi diffusion (Redi, 1982) and the Gent-McWilliams parameterization (Gent and McWilliams, 1990) in the tracer equations. In regions with a resolution between 25 and 50 km, isopycnal and diapycnal diffusivities are scaled linearly with resolution. Below a resolution of 25 km, the parameterized diffusivity is set to a small value as it is assumed that eddy fluxes are resolved. This assumption does, however, not hold everywhere as the grid is not eddy resolving on the shelves and in the Fram Strait (Wekerle et al., 2017b). Consequently, the diffusivity is on the low side in the model in these places where the Rossby radius of deformation is small relative to the grid resolution. One consequence of the low diffusivity is that the riverine supplied DSI is trapped on the shelves, rather than being mixed outwards to the deep parts of the Arctic Ocean. This is especially clear on the Russian shelves where the DSI concentration is high close to the coast (Fig. 6a and c), with a sharp gradient towards the central Arctic due to the low diapycnal mixing. This artifact contributes to the low modeled DSI in the central Arctic.

Providing eddy resolving resolution for the whole Arctic Ocean is currently not feasible for our setup due to computational constraints, but a run utilizing a grid with a 1 km resolution in the Fram Strait shows promising results in the area regarding the recirculation branch of the Atlantic water and the eddy kinetic energy (Wekerle et al., 2017a). The current 4.5 km setup is thus a benchmark setup, from which we can develop future grids for specific questions, and serves to highlight where a higher resolution would be beneficial.

5. Conclusion

We have presented the first global ocean general circulation biogeochemical model (OGCBM) with an Arctic-wide horizontal resolution of 4.5 km, and analyzed the results for the years 2011 to 2015. The average pan-Arctic NPP sums up to 445 Tg C yr^{-1} , which is in the middle of the range of previous studies from both OGCBMs and satellite-based estimates. Most of the modeled production takes place in the inflow regions of the Greenland, Barents and Chukchi Seas where both nutrient and light availability is highest on average. On the Siberian and Beaufort Sea shelves, the average productivity is low, with somewhat higher values in the coastal regions where the modeled ice breaks up the earliest and nutrients are supplied from rivers. On average, 20% of the production takes place under the ice, while 12% is associated with the marginal ice zone (MIZ). The model produces a surface nutrient gradient across the Arctic Ocean, with relatively high concentrations in the North Atlantic and Pacific Oceans, intermediate concentrations in the central Arctic beneath the ice and lowest in the Beaufort Gyre, similar to *in situ* observations. Light limitation dominates in the beginning of the summer season, but with time, nutrients are exhausted in the surface ocean, and nutrient limitation becomes more pronounced in all regions, except for the northernmost central Arctic,

where light limitation is the main controller of growth the whole year. The surface nutrient limitation means that a subsurface chlorophyll maximum (SCM) develops in most areas of the Arctic Ocean, following the nutricline downwards until light limitation dominates. The duration of the SCM ranges from two weeks in the northernmost areas to more than four months in coastal areas of the Barents Sea in the model. A caveat in the model run is the low inflow of dissolved inorganic silicon (DSi) from the North Pacific, leading to a low DSi concentration in the Canada Basin, which possibly affects the total NPP as well as the SCM.

The high resolution means that the currents are well defined and characterized by filaments. The presence of eddies and small scale fronts induce a patchiness in the spatial distribution of the surface chlorophyll and NPP, as also observed in reality. This is especially the case in the Nordic Seas where the model resolution is relatively high compared to the Rossby radius. Towards the north, the sea ice is fragmented compared to models of coarser resolution, thereby allowing for a more heterogeneous light penetration, something that will become increasingly important to capture as the Arctic sea ice becomes younger, thinner and more fragmented.

All in all, FESOM-RECOM2 performs well in the high resolution setup, and is well suited for future studies of the Arctic Ocean, with the special strength of the model being that it can be used to investigate processes on a different spatial scale than most global OGCBMs.

Declarations of interest

Declarations of interest: none.

Acknowledgements

We would like to thank the FESOM team at the Alfred Wegener Institute for support and discussions regarding this study, as well as the FRAM community, and especially Eva-Maria Nöthig, for discussions concerning the realism of the model results. We would also like to thank the two anonymous reviewers for their comments, which significantly improved the manuscript. V. Schourup-Kristensen and C. Wekerle are funded by the FRontiers in Arctic marine Monitoring program (FRAM). Computational resources were made available by the Norddeutscher Verbund für Hoch- und Höchstleistungsrechnen (HLRN). The model data in this study is available upon request (schourup@awi.de).

Appendix A. Supplementary material

Supplementary data associated with this article can be found, in the online version, at <https://doi.org/10.1016/j.pocean.2018.09.006>.

References

- Arndt, S., Nicolaus, M., 2014. Seasonal cycle and long-term trend of solar energy fluxes through Arctic sea ice. *Cryosphere* 8, 2219–2233. <https://doi.org/10.5194/tc-8-2219-2014>.
- Arrigo, K.R., van Dijken, G.L., 2015. Continued increases in arctic ocean primary production. *Progr. Oceanogr.* 136, 60–70. <https://doi.org/10.1016/j.pocean.2015.05.002>.
- Arrigo, K.R., van Dijken, G.L., Bushinsky, S., 2008. Primary production in the Southern Ocean, 1997–2006. *J. Geophys. Res.* 113. <https://doi.org/10.1029/2007JC004551>.
- Arrigo, K.R., Matrai, P.A., van Dijken, G.L., 2011. Primary productivity in the Arctic Ocean: impacts of complex optical properties and subsurface chlorophyll maxima on large-scale estimates. *J. Geophys. Res.* 116, L08304–15. <https://doi.org/10.1029/2011JC007273>.
- Arrigo, K.R., Perovich, D.K., Pickart, R.S., Brown, Z.W., van Dijken, G.L., Lowry, K.E., Mills, M.M., Palmer, M.A., Balch, W.M., Bahr, F., Bates, N.R., Benitez-Nelson, C., Bowler, B., Brownlee, E., Ehn, J.K., Frey, K.E., Garley, R., Laney, S.R., Lubelczyk, L., Mathis, J., Matsuoka, A., Mitchell, B.G., Moore, G.W.K., Ortega-Retuerta, E., Pal, S., Polashenski, C.M., Reynolds, R.A., Schieber, B., Sosik, H.M., Stephens, M., Swift, J.H., 2012. Massive phytoplankton blooms under arctic sea ice. *Science* 336, 1408. <https://doi.org/10.1126/science.1215065>.
- Arrigo, K.R., Perovich, D.K., Pickart, R.S., Brown, Z.W., van Dijken, G.L., Lowry, K.E., Mills, M.M., Palmer, M.A., Balch, W.M., Bates, N.R., Benitez-Nelson, C.R., Brownlee, E., Frey, K.E., Laney, S.R., Mathis, J., Matsuoka, A., Mitchell, B.G., Moore, G.W.K., Reynolds, R.A., Sosik, H.M., Swift, J.H., 2014. Phytoplankton blooms beneath the ice in the Chukchi Sea. *Deep-Sea Res. Pt. II* 105, 1–16. <https://doi.org/10.1016/j.dsr2.2014.03.018>.
- Assmy, P., Fernandez-Mendez, M., Duarte, P., Meyer, A., Randelhoff, A., Mundy, C.J., Olsen, L.M., Kauko, H.M., Bailey, A., Chierici, M., Cohen, L., Dougligeris, A.P., Ehn, J.K., Fransson, A., Gerland, S., Hop, H., Hudson, S.R., Hughes, N., Itkin, P., Johnsen, G., King, J.A., Koch, B.P., Koenig, Z., Kwasiński, S., Laney, S.R., Nicolaus, M., Pavlov, A.K., Polashenski, C.M., Provost, C., Rösel, A., Sandbu, M., Spreen, G., Smedsrud, L.H., Sundfjord, A., Taskjelle, T., Tatarek, A., Wiktor, J., Wagner, P.M., Wold, A., Steen, H., Granskog, M.A., 2017. Leads in Arctic pack ice enable early phytoplankton blooms below snow-covered sea ice. *Sci. Rep.* 1–9. <https://doi.org/10.1038/srep40850>.
- Aumont, O., Bopp, L., 2006. Globalizing results from ocean in situ iron fertilization studies. *Global Biogeochem. Cycles* 20. <https://doi.org/10.1029/2005GB002591>.
- Bebieva, Y., Timmermans, M.-L., 2016. An examination of double-diffusive processes in a mesoscale eddy in the Arctic Ocean. *J. Geophys. Res.* 121, 457–475. <https://doi.org/10.1002/2015JC011105>.
- Behrenfeld, M.J., 2005. Carbon-based ocean productivity and phytoplankton physiology from space. *Global Biogeochem. Cy.* 19. <https://doi.org/10.1029/2004GB002299>.
- Behrenfeld, M.J., Falkowski, P.G., 1997. Photosynthetic rates derived from satellite-based chlorophyll concentration. *Limnol. Oceanogr.* 42, 1–20. <https://doi.org/10.4319/lo.1997.42.1.0001>.
- Bernard, C.Y., Dürr, H.H., Heinze, C., Segsneider, J., Maier-Reimer, E., 2011. Contribution of riverine nutrients to the silicon biogeochemistry of the global ocean – a model study. *Biogeosciences* 8, 551–564. <https://doi.org/10.5194/bg-8-551-2011>.
- Beusen, A.H.W., Bouwman, A.F., Dürr, H.H., Dekkers, A.L.M., Hartmann, J., 2009. Global patterns of dissolved silica export to the coastal zone: Results from a spatially explicit global model. *Global Biogeochem. Cy.* 23. <https://doi.org/10.1029/2008GB003281>.
- Boetius, A., Albrecht, S., Bakker, K., Bienhold, C., Felden, J., Fernandez-Mendez, M., Hendricks, S., Katlein, C., Lalande, C., Krumpen, T., Nicolaus, M., Peeken, I., Rabe, B., Rogacheva, A., Rybakova, E., Somavilla, R., Wenzhöfer, F., 2013. Export of algal biomass from the melting Arctic sea ice. *Science* 339, 1430–1432. <https://doi.org/10.1126/science.1231346>.
- Brown, Z.W., Lowry, K.E., Palmer, M.A., van Dijken, G.L., Mills, M.M., Pickart, R.S., Arrigo, K.R., 2015. Characterizing the subsurface chlorophyll a maximum in the Chukchi Sea and Canada Basin. *Deep-Sea Res. Part II* 118, 88–104. <https://doi.org/10.1016/j.dsr2.2015.02.010>.
- Carmack, E., Barber, D., Christensen, J., Macdonald, R., Rudels, B., Sakshaug, E., 2006. Climate variability and physical forcing of the food webs and the carbon budget on panarctic shelves. *Progr. Oceanogr.* 71, 145–181. <https://doi.org/10.1016/j.pocean.2006.10.005>.
- Carmack, E., Chapman, D.C., 2003. Wind-driven shelf/basin exchange on an Arctic shelf: the joint roles of ice cover extent and shelf-break bathymetry. *Geophys. Res. Lett.* 30. <https://doi.org/10.1029/2003GL017526>. 47–4.
- Carr, M.-E., Friedrichs, M.A.M., Schmeltz, M., Noguchi Aita, M., Antoine, D., Arrigo, K.R., Asanuma, I., Aumont, O., Barber, R., Behrenfeld, M., Bidigare, R., Buitenhuis, E.T., Campbell, J., Ciotti, A., Dierssen, H., Dowell, M., Dunne, J., Esaias, W., Gentili, B., Gregg, W., Groom, S., Hoepffner, N., Ishizaka, J., Kameda, T., Le Quééré, C., Lohrenz, S., Marra, J., Mélin, F., Moore, K., Morel, A., Reddy, T.E., Ryan, J., Scardi, M., Smyth, T., Turpie, K., Tilstone, G., Waters, K., Yamanaka, Y., 2006. A comparison of global estimates of marine primary production from ocean color. *Deep Sea Res. Pt. II* 53, 741–770. <https://doi.org/10.1016/j.dsr2.2006.01.028>.
- Cavaliere, D.J., Parkinson, C.L., Gloersen, P., Zwally, H.J., 1996. updated yearly, accessed 15.03.17. Sea ice concentrations from Nimbus-7 SMMR and DMSP SSM/I-SSMIS passive microwave data, version 1., 2011 to 2015. doi:<https://doi.org/10.5067/8GQ8LZQVLOVL>.
- Chaves, J.E., Werdell, P.J., Proctor, C.W., Neeley, A.R., Freeman, S.A., Thomas, C.S., Hooker, S.B., 2015. Assessment of ocean color data records from MODIS-Aqua in the western Arctic Ocean. *Deep-Sea Res. Pt. II* 118, 32–43. <https://doi.org/10.1016/j.dsr2.2015.02.011>.
- Chen, C., Gao, G., Zhang, Y., Beardsley, R.C., Lai, Z., Qi, J., Lin, H., 2016. Circulation in the Arctic Ocean: results from a high-resolution coupled ice-sea nested Global-FVCOM and Arctic-FVCOM system. *Progr. Oceanogr.* 141, 60–80. <https://doi.org/10.1016/j.pocean.2015.12.002>.
- Cherkasheva, A., Nöthig, E.M., Bauerfeind, E., Melsheimer, C., Bracher, A., 2013. From the chlorophyll a in the surface layer to its vertical profile: a Greenland Sea relationship for satellite applications. *Ocean Sci.* 9, 431–445. <https://doi.org/10.5194/os-9-431-2013>.
- Codispoti, L.A., Kelly, V., Thessen, A., Matrai, P., Suttles, S., Hill, V., Steele, M., Light, B., 2013. Synthesis of primary production in the Arctic Ocean: III. Nitrate and phosphate based estimates of net community production. *Progr. Oceanogr.* 110, 126–150. <https://doi.org/10.1016/j.pocean.2012.11.006>.
- Comiso, J.C., 2012. Large decadal decline of the arctic multiyear ice cover. *J. Climate* 25, 1176–1193. <https://doi.org/10.1175/JCLI-D-11-00113.1>.
- Cullen, J.J., 2015. Subsurface chlorophyll maximum layers: enduring enigma or mystery solved? *Annu. Rev. Mar. Sci.* 7, 207–239. <https://doi.org/10.1146/annurev-marine-010213-135111>.
- Davis, P.E.D., Lique, C., Johnson, H.L., Guthrie, J.D., 2016. Competing effects of elevated vertical mixing and increased freshwater input on the stratification and sea ice cover in a changing arctic ocean. *J. Phys. Oceanogr.* 46, 1531–1553. <https://doi.org/10.1175/JPO-D-15-0174.1>.
- Deal, C.J., Steiner, N., Christian, J., Kinney, J.C., Denman, K.L., Elliott, S.M., Gibson, G., Jin, M., Lavoie, D., Lee, S.H., Lee, W., Maslowski, W., Wang, J., Watanabe, E., 2014. Progress and challenges in biogeochemical modeling of the Pacific Arctic region. In: *The Pacific Arctic Region*. Springer, pp. 393–445.
- Dürr, H.H., Meybeck, M., Hartmann, J., Laruelle, G.G., Roubeix, V., 2011. Global spatial distribution of natural riverine silica inputs to the coastal zone. *Biogeosciences* 8,

- 597–620. <https://doi.org/10.5194/bg-8-597-2011>.
- Engelsen, O., Hop, H., Hegseth, E.N., Hansen, E., Falk-Petersen, S., 2004. Deriving phytoplankton biomass in the Marginal Ice Zone from satellite observable parameters. *Rem. Sens.* 25, 1453–1457. <https://doi.org/10.1080/0143116031000159243>.
- Erga, S.R., Seebiyonga, N., Hamre, B., Frette, Ø., Hovland, E., Hancke, K., Drinkwater, K., Rey, F., 2014. Environmental control of phytoplankton distribution and photosynthetic performance at the Jan Mayen Front in the Norwegian Sea. *J. Marine Syst.* 130, 193–205. <https://doi.org/10.1016/j.jmarsys.2012.01.006>.
- Fernández-Méndez, M., Katlein, C., Rabe, B., Nicolaus, M., Peeken, I., Bakker, K., Flores, H., Boetius, A., 2015. Photosynthetic production in the central Arctic Ocean during the record sea-ice minimum in 2012. *Biogeosciences* 12, 3525–3549. <https://doi.org/10.5194/bg-12-3525-2015>.
- Frey, K.E., Perovich, D.K., Light, B., 2011. The spatial distribution of solar radiation under a melting Arctic sea ice cover. *Geophys. Res. Lett.* 38. <https://doi.org/10.1029/2011GL049421>.
- García, H.E., Locarnini, R.A., Boyer, T.P., & Antonov, J.I. 2006. Volume 4: Nutrients (phosphate, nitrate, silicate). In: Levitus, S. (Ed.), *World Ocean Atlas 2005* (p. 396). NOAA Atlas NESDIS 64, U.S. Government Printing Office, Washington, D.C.
- García, H.E., Locarnini, R.A., Boyer, T.P., Antonov, J.I., Baranova, O.K., Zweng, M.M., Reagan, J.R., Johnson, D.R., 2014. *World ocean atlas 2013*, volume 4: Dissolved inorganic nutrients (phosphate, nitrate, silicate). URL <https://doi.org/10.7265/N5QJ7F7W>.
- Gent, P., McWilliams, J., 1990. Isopycnal mixing in ocean circulation models. *J. Phys. Oceanogr.* 20, 150–155.
- Gosselin, M., Levasseur, M., Wheeler, P.A., 1997. New measurements of phytoplankton and ice algal production in the Arctic Ocean. *Deep Sea Res. Pt. II* 44, 1623–1644. [https://doi.org/10.1016/S0967-0645\(97\)00054-4](https://doi.org/10.1016/S0967-0645(97)00054-4).
- Hattermann, T., Isachsen, P.E., Appen, W.J., 2016. Eddy-driven recirculation of Atlantic Water in Fram Strait. *Geophys. Res. Lett.* [https://doi.org/10.1002/\(ISSN\)1944-8007](https://doi.org/10.1002/(ISSN)1944-8007).
- Hauk, J., Völker, C., 2015. Rising atmospheric CO₂ leads to large impact of biology on southern ocean CO₂ uptake via changes of the Revelle factor. *Geophys. Res. Lett.* 42, 1459–1464. <https://doi.org/10.1002/2015GL063070>.
- Hauk, J., Völker, C., Wang, T., Hoppema, M., Losch, M., Wolf-Gladrow, D.A., 2013. Seasonally different carbon flux changes in the Southern Ocean in response to the southern annular mode. *Global Biogeochem. Cy.* 27, 1236–1245.
- Heiskanen, A.S., Review, A.K.O.L., 1996. Distribution and sinking rates of phytoplankton, detritus, and particulate biogenic silica in the Laptev Sea and Lena River (Arctic Siberia). *Mar. Chem.* 229–245 1997.
- Hill, V.J., Matrai, P.A., Olson, E., Suttles, S., Steele, M., Codispoti, L.A., Zimmerman, R.C., 2013. Synthesis of integrated primary production in the Arctic Ocean: II. In situ and remotely sensed estimates. *Prog. Oceanogr.* 110, 107–125. <https://doi.org/10.1016/j.pocean.2012.11.005>.
- Japan Meteorological Agency, J., 2013, accessed March 2016. JRA-55: Japanese 55-year reanalysis, daily 3-hourly and 6-hourly data. URL <https://doi.org/10.5065/D6HH6H41>.
- Jin, M., Deal, C., Lee, S.H., Elliott, S., Hunke, E., Maltrud, M., Jeffery, N., 2012. Investigation of arctic sea ice and ocean primary production for the period 1992–2007 using a 3-d global ice-ocean ecosystem model. *Deep-Sea Res. Pt. II* 28–35. <https://doi.org/10.1016/j.dsr2.2011.06.003>.
- Jin, M., Popova, E.E., Zhang, J., Ji, R., Pendleton, D., Varpe, Ø., Yool, A., Lee, Y.J., 2016. Ecosystem model intercomparison of under-ice and total primary production in the Arctic Ocean. *J. Geophys. Res.* 121, 934–948. <https://doi.org/10.1002/2015JC011183>.
- Katlein, C., Arndt, S., Nicolaus, M., Perovich, D.K., Jakuba, M.V., Suman, S., Elliott, S., Whitcomb, L.L., McFarland, C.J., Gerdes, R., Boetius, A., German, C.R., 2015. Influence of ice thickness and surface properties on light transmission through Arctic sea ice. *J. Geophys. Res.* 120, 5932–5944. <https://doi.org/10.1002/2015JC010914>.
- Key, R.M., Kozyr, A., Sabine, C.L., Lee, K., Wanninkhof, R., Bullister, J.L., Feely, R.A., Millero, F.J., Mordy, C., Peng, T.-H., 2004. A global ocean carbon climatology: results from global data analysis project (GLODAP). *Global Biogeochem. Cy.* 18. <https://doi.org/10.1029/2004GB002247>.
- Lamarque, J.F., Bond, T.C., Eyring, V., Granier, C., Heil, A., Klimont, Z., Lee, D., Liousse, C., Mieville, A., Owen, B., Schultz, M.G., Shindell, D., Smith, S.J., Stehfest, E., Van Aardenne, J., Cooper, O.R., Kainuma, M., Mahowald, N., McConnell, J.R., Naik, V., Riahi, K., van Vuuren, D.P., 2010. Historical (1850–2000) gridded anthropogenic and biomass burning emissions of reactive gases and aerosols: methodology and application. *Atmos. Chem. Phys.* 10, 7017–7039. <https://doi.org/10.5194/acp-10-7017-2010>.
- Large, W.G., McWilliams, J.C., Doney, S.C., 1994. Oceanic vertical mixing: a review and a model with a nonlocal boundary layer parameterization. *Rev. Geophys.* 32, 363–403.
- Large, W.G., Yeager, S.G., 2008. The global climatology of an interannually varying air–sea flux data set. *Clim. Dynam.* 33, 341–364. <https://doi.org/10.1007/s00382-008-0441-3>.
- Le Fouest, V., Babin, M., Tremblay, J.É., 2013. The fate of riverine nutrients on Arctic shelves. *Biogeosciences* 10, 3661–3677. <https://doi.org/10.5194/bg-10-3661-2013>.
- Létolite, R., Martin, J.M., Thomas, A.J., Gordeev, V.V., 1993. ¹⁸O abundance and dissolved silicate in the Lena delta and Laptev Sea (Russia). *Mar. Chem.* 43, 47–64. [https://doi.org/10.1016/0304-4203\(93\)90215-a](https://doi.org/10.1016/0304-4203(93)90215-a).
- Losch, M., Strass, V., Cisewski, B., Klaas, C., Bellerby, R.G., 2014. Ocean state estimation from hydrography and velocity observations during EIFEX with a regional biogeochemical ocean circulation model. *J. Mar. Sys.* 129, 437–451. <https://doi.org/10.1016/j.jmarsys.2013.09.003>.
- Lowry, K.E., van Dijken, G.L., Arrigo, K.R., 2014. Evidence of under-ice phytoplankton blooms in the Chukchi Sea from 1998 to 2012. *Deep-Sea Res. Pt. II* 105, 105–117. <https://doi.org/10.1016/j.dsr2.2014.03.013>.
- Lumpkin, R., Johnson, G.C., 2013. Global ocean surface velocities from drifters: mean, variance, El Niño–Southern Oscillation response, and seasonal cycle. *J. Geophys. Res.: Oceans* 118, 2992–3006. <https://doi.org/10.1002/jgrc.20210>.
- Mahadevan, A., 2016. The impact of submesoscale physics on primary productivity of plankton. *Ann. Rev. Mar. Sci.* 8, 161–184. <https://doi.org/10.1146/annurev-marine-010814-015912>.
- Martin, A.P., 2003. Phytoplankton patchiness: the role of lateral stirring and mixing. *Prog. Oceanogr.* 57, 125–174. [https://doi.org/10.1016/S0079-6611\(03\)00085-5](https://doi.org/10.1016/S0079-6611(03)00085-5).
- Martin, J., Tremblay, J.É., Price, N.M., 2012. Nutritive and photosynthetic ecology of subsurface chlorophyll maxima in Canadian Arctic waters. *Biogeosciences* 9, 5353–5371. <https://doi.org/10.5194/bg-9-5353-2012>.
- Matsuoka, A., Huot, Y., Shimada, K., Saitoh, S.I., 2007. Bio-optical characteristics of the western Arctic Ocean: implications for ocean color algorithms. *Can. J. Rem. Sens.* 33, 503–518. <https://doi.org/10.5589/m07-059>.
- Mayorga, E., Seitzinger, S.P., Harrison, J.A., Dumont, E., Beusen, A.H., Bouwman, A., Fekete, B.M., Kroeze, C., Van Drecht, G., 2010. Global nutrient export from watersheds 2 (news 2): model development and implementation. *Environ. Model. Softw.* 25, 837–853. <https://doi.org/10.1016/j.envsoft.2010.01.007>.
- McKiver, W.J., Vichi, M., Lovato, T., Storto, A., Masina, S., 2015. Impact of increased grid resolution on global marine biogeochemistry. *J. Mar. Sys.* 147, 153–168. <https://doi.org/10.1016/j.jmarsys.2014.10.003>.
- McLaughlin, F.A., Carmack, E.C., 2010. Deepening of the nutricline and chlorophyll maximum in the Canada Basin interior, 2003–2009. *Geophys. Res. Lett.* 37, n/a–n/a. <https://doi.org/10.1029/2010GL045459>.
- Mosharov, S.A., 2010. Distribution of the primary production and chlorophyll a in the Kara Sea in September of 2007. *Oceanology* 50, 884–892. <https://doi.org/10.1134/S0001437010060081>.
- Mundy, C.J., Gosselin, M., Ehn, J., Gratton, Y., Rossnagel, A., Barber, D.G., Martin, J., Tremblay, J.-É., Palmer, M., Arrigo, K.R., Darnis, G., Fortier, L., Else, B., Papakyriakou, T., 2009. Contribution of under-ice primary production to an ice-edge upwelling phytoplankton bloom in the Canadian Beaufort Sea. *Geophys. Res. Lett.* 36, L17601–5. <https://doi.org/10.1029/2009GL038837>.
- Nicolaus, M., Katlein, C., Maslanik, J., Hendricks, S., 2012. Changes in Arctic sea ice result in increasing light transmittance and absorption. *Geophys. Res. Lett.* 39. <https://doi.org/10.1029/2012GL053738>.
- Nishino, S., Itoh, M., Kawaguchi, Y., Kikuchi, T., Aoyama, M., 2011. Impact of an unusually large warm-core eddy on distributions of nutrients and phytoplankton in the southwestern Canada Basin during late summer/early fall 2010. *Geophys. Res. Lett.* 38. <https://doi.org/10.1029/2011GL047885>.
- Nurser, A.J.G., Bacon, S., 2014. The Rossby radius in the Arctic Ocean. *Ocean Sci.* 10, 967–975. <https://doi.org/10.5194/os-10-967-2014>.
- Olli, K., Wassmann, P., Reigstad, M., Ratkova, T.N., Arashkevich, E., Pasternak, A., Matrai, P.A., Knulst, J., Tranvik, L., Klais, R., Jacobsen, A., 2007. The fate of production in the central Arctic Ocean – top–down regulation by zooplankton expatriates? *Prog. Oceanogr.* 72, 84–113. <https://doi.org/10.1016/j.pocean.2006.08.002>.
- Oziel, L., Neukermans, G., Ardyna, M., Lancelot, C., Tison, J.L., Wassmann, P., Sirven, J., Ruiz-Pino, D., Gascard, J.C., 2017. Role for Atlantic inflows and sea ice loss on shifting phytoplankton blooms in the Barents Sea. *J. Geophys. Res.: Oceans* 122, 5121–5139. <https://doi.org/10.1002/2016JC012582>.
- Pabi, S., van Dijken, G.L., Arrigo, K.R., 2008. Primary production in the Arctic Ocean, 1998–2006. *J. Geophys. Res.* 113, C08005–22. <https://doi.org/10.1029/2007JC004578>.
- Pacanowski, R.C., Philander, S., 1981. Parameterization of vertical mixing in numerical models of tropical oceans. *J. Phys. Oceanogr.* 11, 1443–1451.
- Packard, T.T., Codispoti, L.A., 2007. Respiration, mineralization, and biochemical properties of the particulate matter in the southern Russian Basin water column in April 1981. *Deep Sea Res. Pt. I* 54, 403–414. <https://doi.org/10.1016/j.dsr.2006.12.008>.
- Perovich, D.K., Jones, K.F., Light, B., Eicken, H., 2011. Solar partitioning in a changing Arctic sea-ice cover. *Ann. Glaciol.* 52, 192–196. <https://doi.org/10.3189/172756411795931543>.
- Perrette, M., Yool, A., Quartly, G.D., Popova, E.E., 2011. Near-ubiquity of ice-edge blooms in the Arctic. *Biogeosciences* 8, 515–524. <https://doi.org/10.5194/bg-8-515-2011>.
- Popova, E.E., Yool, A., Coward, A.C., Aksenov, Y.K., Alderson, S.G., de Cuevas, B.A., Anderson, T.R., 2010. Control of primary production in the Arctic by nutrients and light: insights from a high resolution ocean general circulation model. *Biogeosciences* 7, 3569–3591.
- Popova, E.E., Yool, A., Coward, A.C., Dupont, F., Deal, C., Elliott, S., Hunke, E., Jin, M., Steele, M., Zhang, J., 2012. What controls primary production in the Arctic Ocean? results from an intercomparison of five general circulation models with biogeochemistry. *J. Geophys. Res.* 117. <https://doi.org/10.1029/2011JC007112>.
- Proshutinsky, A., Aksenov, Y., Clement Kinney, J., Gerdes, R., Golubeva, E., Holland, D., Holloway, G., Jahn, A., Johnson, M., Popova, E., Steele, M., Watanabe, E., 2011. Recent advances in arctic ocean studies employing models from the arctic ocean model intercomparison project. *Oceanography* 24, 102–113. <https://doi.org/10.5670/oceanog.2011.61>.
- Randelhoff, A., Fer, I., Sundfjord, A., Tremblay, J.-É., Reigstad, M., 2016. Vertical fluxes of nitrate in the seasonal nitracline of the Atlantic sector of the Arctic Ocean. *J. Geophys. Res.* 1–14. <https://doi.org/10.1002/2016JC011779>.
- Randelhoff, A., Sundfjord, A., Reigstad, M., 2015. Seasonal variability and fluxes of nitrate in the surface waters over the Arctic shelf slope. *Geophys. Res. Lett.* 42, 3442–3449. <https://doi.org/10.1002/2015GL063655>.
- Redi, M.H., 1982. Oceanic isopycnal mixing by coordinate rotation. *J. Phys. Oceanogr.* 12, 1154–1158.
- Reigstad, M., Wassmann, P., Riser, C.W., 2002. Variations in hydrography, nutrients and chlorophyll a in the marginal ice-zone and the central Barents Sea. *J. Mar. Syst.* 38, 9–29. [https://doi.org/10.1016/S0924-7963\(02\)00167-7](https://doi.org/10.1016/S0924-7963(02)00167-7).

- Sakshaug, E., 2004. Primary and secondary production in the arctic seas. In: Stein, R., MacDonald, R.W. (Eds.), *The Organic Carbon Cycle in the Arctic Ocean*. Springer, Berlin, Heidelberg, pp. 57–81. https://doi.org/10.1007/978-3-642-18912-8_3.
- Schartau, M., Engel, A., Schröter, J., Thoms, S., Völker, C., Wolf-Gladrow, D., 2007. Modelling carbon overconsumption and the formation of extracellular particulate organic carbon. *Biogeosciences* 4, 433–454. <https://doi.org/10.5194/bg-4-433-2007>.
- Schourup-Kristensen, V., Sidorenko, D., Wolf-Gladrow, D.A., Völker, C., 2014. A skill assessment of the biogeochemical model REcoM2 coupled to the Finite Element Sea-Ice Ocean Model (FESOM 1.3). *Geosci. Model Dev.* 7, 2769–2802. <https://doi.org/10.5194/gmd-7-2769-2014>.
- Siegel, D.A., Doney, S.C., Yoder, J.A., 2002. The North Atlantic spring phytoplankton bloom and sverdrup's critical depth hypothesis. *Science* 296, 730–733. <https://doi.org/10.1126/science.1069174>.
- Sorokin, Y.L., Sorokin, P.Y., 1996. Plankton and primary production in the Lena River estuary and in the south-eastern Laptev Sea. *Estuar. Coast. Shelf Sci.* 43, 399–418. <https://doi.org/10.1006/ecss.1996.0078>.
- Spall, M.A., Pickart, R.S., Fratantoni, P.S., Plueddemann, A.J., 2008. Western arctic shelfbreak eddies: formation and transport. *J. Phys. Oceanogr.* 38, 1644–1668. <https://doi.org/10.1175/2007JPO3829.1>.
- Steiner, N.S., Sou, T., Deal, C., Jackson, J.M., Jin, M., Popova, E., Williams, W., Yool, A., 2016. The future of the subsurface chlorophyll-a maximum in the Canada Basin-A model intercomparison. *J. Geophys. Res.* 121, 387–409. <https://doi.org/10.1002/2015JC011232>.
- Stroeve, J.C., Serreze, M.C., Holland, M.M., Kay, J.E., Malanik, J., Barrett, A.P., 2012. The arctic's rapidly shrinking sea ice cover: a research synthesis. *Clim. Change* 110, 1005–1027. <https://doi.org/10.1007/s10584-011-0101-1>.
- Taylor, M.H., Losch, M., Bracher, A., 2013a. On the drivers of phytoplankton blooms in the antarctic marginal ice zone: a modeling approach. *J. Geophys. Res.* 118, 63–75. <https://doi.org/10.1029/2012JC008418>.
- Taylor, R.L., Semeniuk, D.M., Payne, C.D., Zhou, J., Tremblay, J.-É., Cullen, J.T., Maldonado, M.T., 2013b. Colimitation by light, nitrate, and iron in the Beaufort Sea in late summer. *J. Geophys. Res.* 118, 3260–3277. <https://doi.org/10.1002/jgrc.20244>.
- Torres-Valdés, S., Tsubouchi, T., Bacon, S., Naveira-Garabato, A.C., Sanders, R., McLaughlin, F.A., Petrie, B., Kattner, G., Azetsu-Scott, K., Whitledge, T.E., 2013. Export of nutrients from the Arctic Ocean. *J. Geophys. Res.* 118, 1625–1644. <https://doi.org/10.1002/jgrc.20063>.
- Tremblay, J.-É., Anderson, L.G., Matrai, P., Coupel, P., Bélanger, S., Michel, C., Reigstad, M., 2015. Global and regional drivers of nutrient supply, primary production and CO₂ drawdown in the changing Arctic Ocean. *Progr. Oceanogr.* 139, 171–196. <https://doi.org/10.1016/j.pocean.2015.08.009>.
- Tremblay, J.-É., Gagnon, J., 2009. The effects of irradiance and nutrient supply on the productivity of Arctic waters: a perspective on climate change. In: Nihoul, J., Kostianoy, A.G. (Eds.), *Influence of Climate Change on the Changing Arctic and Sub-Arctic Conditions*. Springer Science & Business Media, pp. 73–93. https://doi.org/10.1007/978-1-4020-9460-6_7.
- Tremblay, J.-É., Raimbault, P., Garcia, N., Lansard, B., Babin, M., Gagnon, J., 2014. Impact of river discharge, upwelling and vertical mixing on the nutrient loading and productivity of the Canadian Beaufort Shelf. *Biogeosciences* 11, 4853–4868. <https://doi.org/10.5194/bg-11-4853-2014>.
- Tremblay, J.-É., Simpson, K., Martin, J., Miller, L., Gratton, Y., Barber, D., Price, N.M., 2008. Vertical stability and the annual dynamics of nutrients and chlorophyll fluorescence in the coastal, southeast Beaufort Sea. *J. Geophys. Res.* 113. <https://doi.org/10.1029/2007JC004547>.
- Vancoppenolle, M., Bopp, L., Madec, G., Dunne, J.P., Ilyina, T., Halloran, P.R., Steiner, N., 2013. Future Arctic Ocean primary productivity from CMIP5 simulations: uncertain outcome, but consistent mechanisms. *Glob. Biogeochem. Cy.* 27, 605–619. <https://doi.org/10.1002/gbc.20055>.
- Varela, D.E., Crawford, D.W., Wrohan, I.A., Wyatt, S.N., Carmack, E.C., 2013. Pelagic primary productivity and upper ocean nutrient dynamics across Subarctic and Arctic Seas. *J. Geophys. Res.* 118, 7132–7152. <https://doi.org/10.1002/2013JC009211>.
- Vedernikov, V., Demidov, A., Sud'bin, A., 1995. Primary production and chlorophyll in the Kara Sea in september 1993. *Oceanology* 34, 630–640.
- Vernet, M., 1991. Phytoplankton dynamics in the Barents Sea estimated from chlorophyll budget models. *Polar Res.* 10, 129–146. <https://doi.org/10.3402/polar.v10i1.6733>.
- Wang, J., 2005. Absorption and backscattering in the Beaufort and Chukchi Seas. *J. Geophys. Res.* 110. <https://doi.org/10.1029/2002JC001653>.
- Wang, Q., Danilov, S., Jung, T., Kaleschke, L., Wernecke, A., 2016a. Sea ice leads in the Arctic Ocean: model assessment, interannual variability and trends. *Geophys. Res. Lett.* 43, 7019–7027. <https://doi.org/10.1002/2016GL068696>.
- Wang, Q., Danilov, S., Sidorenko, D., Timmermann, R., Wekerle, C., Wang, X., Jung, T., Schröter, J., 2014. The finite element sea ice-ocean model (FESOM) v.1.4: formulation of an ocean general circulation model. *Geosci. Model Dev.* 7, 663–693. <https://doi.org/10.5194/gmd-7-663-2014>.
- Wang, Q., Ilicak, M., Gerdes, R.d., Drange, H., Aksenov, Y., Bailey, D.A., Bentsen, M., Biastoch, A., Bozec, A., ning, C.B., Cassou, C., Chassignet, E., Coward, A.C., Curry, B., Danabasoglu, G., Danilov, S., Fernandez, E., Fogli, P.G., Fujii, Y., Griffies, S.M., Iovino, D., Jahn, A., Jung, T., Large, W.G., Lee, C., Lique, C., Lu, J., Masina, S., Nurser, A.J.G., Rabe, B., Roth, C., lia, D.S. y. M., Samuels, B.L., Spence, P., Tsujino, H., Valcke, S., Voldoire, A., Wang, X., Yeager, S.G., 2016b. An assessment of the Arctic Ocean in a suite of interannual CORE-II simulations. Part I: Sea ice and solid freshwater. *Oce. Mod.* 99, 110–132. <https://doi.org/10.1016/j.ocemod.2015.12.008>.
- Wassmann, P., 2011. Arctic marine ecosystems in an era of rapid climate change. *Progr. Oceanogr.* 90, 1–17. <https://doi.org/10.1016/j.pocean.2011.02.002>.
- Wassmann, P., Slagstad, D., Riser, C.W., Reigstad, M., 2006. Modelling the ecosystem dynamics of the Barents Sea including the marginal ice zone. *J. Mar. Sys.* 59, 1–24. <https://doi.org/10.1016/j.jmarsys.2005.05.006>.
- Watanabe, E., Onodera, J., Harada, N., Honda, M.C., Kimoto, K., Kikuchi, T., Nishino, S., Matsuno, K., Yamaguchi, A., Ishida, A., Kishi, M.J., 2014. Enhanced role of eddies in the Arctic marine biological pump. *Nat. Comm.* 5. <https://doi.org/10.1038/ncomms4950>.
- Wekerle, C., Wang, Q., von Appen, W.-J., Danilov, S., Schourup-Kristensen, V., Jung, T., 2017a. Eddy-resolving simulation of the Atlantic Water circulation in the Fram Strait with focus on the seasonal cycle. *J. Geophys. Res.* <https://doi.org/10.1002/2017JC012974>.
- Wekerle, C., Wang, Q., Danilov, S., Jung, T., Schröter, J., 2013. The Canadian Arctic Archipelago throughflow in a multiresolution global model: Model assessment and the driving mechanism of interannual variability. *J. Geophys. Res.* 118, 4525–4541. <https://doi.org/10.1002/jgrc.20330>.
- Wekerle, C., Wang, Q., Danilov, S., Schourup-Kristensen, V., von Appen, W.-J., Jung, T., 2017b. Atlantic Water in the Nordic Seas: locally eddy-permitting ocean simulation in a global setup. *J. Geophys. Res.* 1–27. <https://doi.org/10.1002/2016JC012121>.
- Westberry, T., Behrenfeld, M.J., Siegel, D.A., Boss, E., 2008. Carbon-based primary productivity modeling with vertically resolved photoacclimation. *Global Biogeochem. Cy.* 22. <https://doi.org/10.1029/2007GB003078>.
- Williams, W.J., Carmack, E.C., 2008. Combined effect of wind-forcing and isobath divergence on upwelling at Cape Bathurst, Beaufort Sea. *J. Mar. Res.* 66, 645–663. <https://doi.org/10.1357/002224008787536808>.
- Zhang, J., Spitz, Y.H., Steele, M., Ashjian, C., Campbell, R., Berline, L., Matrai, P., 2010. Modeling the impact of declining sea ice on the Arctic marine planktonic ecosystem. *J. Geophys. Res.* 115, C10015. <https://doi.org/10.1029/2009JC005387>.